AFRL-VA-WP-TR-2000-3013

FORMULATION AND APPLICATION OF A STOCHASTIC FATIGUE DAMAGE ACCUMULATION MODEL FOR THE RESPONSE OF BUCKLED COMPOSITE PANELS

P.C. CHEN
D.D. LIU

ZONA TECHNOLOGY, INC.
7430 E. STETSON DRIVE
SUITE 205
SCOTTSDALE, AZ 85251-3540

M.P. MIGNOLET

ARIZONA STATE UNIVERSITY
DEPARTMENT OF MECHANICAL & AEROSPACE ENGINEERING
TEMPE, AZ 85287

MARCH 2000

FINAL REPORT FOR 06/01/1999 – 03/15/2000

AIR VEHICLES DIRECTORATE
AIR FORCE RESEARCH LABORATORY
AIR FORCE MATERIEL COMMAND
WRIGHT-PATTERSON AIR FORCE BASE OH 45433-7542

NOTICE

Using Government drawings, specifications, or other data included in this document for any purpose other than Government procurement does not in any way obligate the U.S. Government. The fact that the Government formulated or supplied the drawings, specifications, or other data does not license the holder or any other person or corporation; or convey any rights or permission to manufacture, use, or sell any patented invention that may relate to them.

This report is releasable to the National Technical Information Service (NTIS). At NTIS, it will be available to the general public, including foreign nations.

THIS TECHNICAL REPORT HAS BEEN REVIEWED AND IS APPROVED FOR PUBLICATION.

Do not return copies of this report unless contractual obligations or notice on a specific document requires its return.

REPORT DOCUMENTATION PAGE	Form Approved OMB No. 0704-0188

1. AGENCY USE ONLY *(Leave blank)*	2. REPORT DATE	3. REPORT TYPE AND DATES COVERED
	MARCH 2000	FINAL REPORT FOR 06/01/1999 - 03/15/2000

4. TITLE AND SUBTITLE
FORMULATION AND APPLICATION OF A STOCHASTIC FATIGUE DAMAGE ACCUMULATION MODEL FOR THE RESPONSE OF BUCKLED COMPOSITE PANELS

5. FUNDING NUMBERS
C F33615-99-C-3203
PE 65502
PR 3005
TA 41
WU A6

6. AUTHOR(S)
P.C. CHEN, D.D. LIU -- ZONA TECHNOLOGY, INC.
M.P. MIGNOLET -- ARIZONA STATE UNIVERSITY

7. PERFORMING ORGANIZATION NAME(S) AND ADDRESS(ES)
ZONA TECHNOLOGY, INC.
7434 E. STETSON DRIVE
SUITE 205
SCOTTSDALE, AZ 85251-3540

8. PERFORMING ORGANIZATION REPORT NUMBER
ZONA 00-09

9. SPONSORING/MONITORING AGENCY NAME(S) AND ADDRESS(ES)
AIR VEHICLES DIRECTORATE
AIR FORCE RESEARCH LABORATORY
AIR FORCE MATERIEL COMMAND
WRIGHT-PATTERSON AFB, OH 45433-7542

10. SPONSORING/MONITORING AGENCY REPORT NUMBER
AFRL-VA-WP-TR-2000-3013

11. SUPPLEMENTARY NOTES
THIS IS A SMALL BUSINESS INNOVATION RESEARCH (SBIR) PHASE I REPORT.

12a. DISTRIBUTION AVAILABILITY STATEMENT
APPROVED FOR PUBLIC RELEASE, DISTRIBUTION UNLIMITED.

12b. DISTRIBUTION CODE

13. ABSTRACT *(Maximum 200 words)*

This report was developed under SBIR contract for topic AF99-269.

This report documents the results of an SBIR Phase I feasibility study on the prediction of the fatigue of composite panels subjected to an extreme environment, i.e. both high temperatures (and temperatures gradients) and a transverse acoustic loading. Of particular interest in this study are situations in which the plate is buckled by the thermal effects and experiences frequent snap-throughs, i.e. excursions from one buckled state to the other. First, a large displacements - small strains structural dynamic formulation is developed that accounts for the given temperature effects and relies on a higher-order shear modeling. Then, a one-mode approximate representation of the panel dynamics is derived that is shown to reduce substantially the complexity of the problem while retaining the essential physics. Next, two equivalent linearization strategies are formulated for the derivation of approximate models of the probability density function of the panel response. Finally, the damage prediction is accomplished by relying on three separate damage scenarios that permit a reliable estimation of the damage in a wide range of conditions, extending specifically from the limiting case of infrequent snap-throughs to the situations in which this behavior dominates the panel response.

14. SUBJECT TERMS
SBIR Report, Postbuckling, Composite Panel, Fatigue Prediction, Thermal Loading, acoustic Excitation, Random Vibration, Equivalent Linearization

15. NUMBER OF PAGES

16. PRICE CODE

17. SECURITY CLASSIFICATION OF REPORT	18. SECURITY CLASSIFICATION OF THIS PAGE	19. SECURITY CLASSIFICATION OF ABSTRACT	20. LIMITATION OF ABSTRACT
UNCLASSIFIED	UNCLASSIFIED	UNCLASSIFIED	SAR

Standard Form 298 (Rev. 2-89) (EG)
Prescribed by ANSI Std. 239.18
Designed using Perform Pro, WHS/DIOR, Oct 94

TABLE OF CONTENTS

LIST OF FIGURES/TABLES

Table | Page

FOREWORD

This report was prepared by ZONA Technology, Inc. the prime contractor, and its team member (Arizona State University) for AFRL, Wright Laboratory, WPAFB, Ohio. It describes the work performed under the Phase I contract of an AF sponsored SBIR No. F33615-99-C-3203 in response to the Topic No. AF99-269 entitled "Formulation and Application of a Stochastic Fatigue Damage Accumulation Model for the Acoustic Response of Buckled Composite Panels." The contractual period was from June 01, 1999 through March 01, 2000. Capt. Michael Spottswood of WL was the technical monitor.

The contributors of this report are: Mr. P.C. Chen (principal investigator), Dr. D.D. Liu of ZONA Technology; Professor M. P. Mignolet and Mr. C.L. Huang of Arizona State University were the ZONA team members.

During the course of the present phase of this research, the technical advice and assistance that the ZONA team received from Capt. Michael Spottswood and Dr. Howard Wolfe of Wright Laboratory are gratefully acknowledged.

SECTION 1

INTRODUCTION

Vibration issues and the associated fatigue accumulation often play a critical role in the design of structural components. This observation is, in particular, true in the context of future supersonic/hypersonic vehicles such as the planned National Aerospace Space Plane (NASP) the skin of which will be subjected to especially harsh operating conditions, e.g. surface temperatures possibly exceeding 3000°F, severe acoustic loading from the engine exhaust, etc. The design of the surface panels appears in this light quite challenging especially since it is not only required to consider each of these environmental factors by itself but it is also necessary to account for their combined effects. As an example of loading interaction, consider the response of panels to the thermal and acoustic excitations mentioned above and note first that the increase of surface temperature will produce compressive stresses in the panels since the extension that they would naturally undergo is prevented by their supports. Further, the magnitude of these stresses, in direct relation to the very large temperature changes, is likely to produce the buckling of some panels.

To sustain such high surface temperatures, specially designed structural materials, such as ceramic matrix composites, will have to be used. The refractory nature of these materials will prevent the heat conduction through the panel and thus will lead to a severe temperature gradient in that direction. The corresponding compressive stresses will exhibit a similar sharp variation through the thickness which will result not only in a normal force but also in a moment that increases the likelihood of buckling (see Ng, 1988, 1989, Lee, 1993, 1997, Vaicaitis, 1994, Moorthy et al. 1995)

Of primary importance in the fatigue damage accumulation process is the *cycling* of the stresses and, thus, buckling represents a specially acute problem if the panel oscillates from its buckled state to its normal configuration, or from one buckled state to another. This latter mechanism, often referred to as snap-through or oil-canning, is especially likely when the panel is subjected, in addition to the thermal loading, to a random transverse excitation such as the acoustic loading from the engine exhaust. The corresponding response of the panel consists of random fluctuations around the buckled position but also often includes large excursions from this configuration, so large in fact that the panel may snap-through to the other buckled state. Accordingly, the goal of the present investigation is the formulation and preliminary assessment of a methodology for the prediction of the fatigue damage accumulated in a panel due to both fluctuations around the buckled states and the snap-throughs.

SECTION 2
PANEL STRUCTURAL DYNAMIC MODELING

The structural dynamic modeling of the panel can be decomposed into two major parts: the composite plate modeling and the derivation of a simplified, one-mode, model both of which are discussed below.

2.1 Composite Plate Modeling

Recent efforts in the structural dynamics of composite plates (see for example Chattopadhyay and Gu, 1994) have emphasized the appropriateness of the higher order plate theory as proposed by Reddy (1987). Specifically, the displacement field inside the plate are selected in the form (see Fig. 2.1)

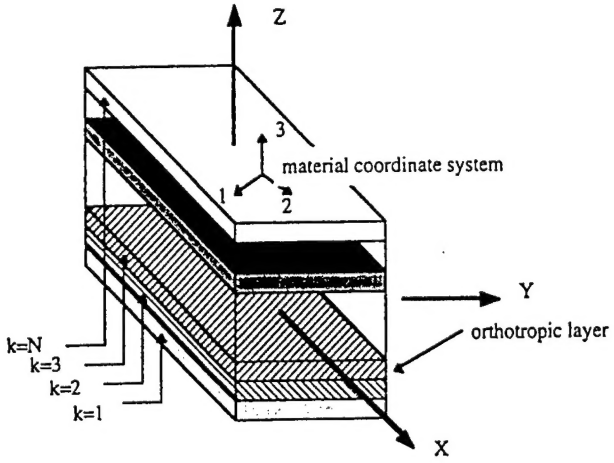

Figure 2.1 Composite plate modeling

$$u(x, y, z, t) = u_0(x, y, t) - z\frac{\partial w_0(x, y, t)}{\partial x} + z\left[1 - \frac{4}{3}\left(\frac{z}{h}\right)^2\right]\varphi_u(x, y, t) \tag{1}$$

$$v(x, y, z, t) = v_0(x, y, t) - z\frac{\partial w_0(x, y, t)}{\partial y} + z\left[1 - \frac{4}{3}\left(\frac{z}{h}\right)^2\right]\varphi_v(x, y, t) \tag{2}$$

$$w(x, y, z, t) = w_0(x, y, t) \tag{3}$$

where u, v, and w are the displacements along the x, y, and z axes, respectively and h denotes the plate thickness. Before proceeding further, it is important to assess the origin of each term present in the above equations.

First, $u_0(x, y, t)$ and $v_0(x, y, t)$ represent the time-varying in-plane displacements of the mid-plane. These displacements are produced by both the thermal effects, which include an overall increase of the panel temperature and temperature gradients along and across the plate, and the mid-plane stretch associated with the large transverse displacements. Note that both of these effects play fundamental roles in the present buckling/postbuckling analysis and thus must absolutely be included in the formulation of the plate equations. Clearly, the thermal effects induce compressive in-plane stresses that

are reflected by an apparent softening of the plate in the transverse direction and consequently facilitate the plate buckling. Once buckling is initiated, the transverse displacements rapidly increase leading to a stretching of the midplate which restores the stiffness of the panel and allows the existence of a stable buckled equilibrium position. Clearly then, one can formally write

$$u_0 = u_0(T, w_0) \qquad \text{and} \qquad v_0 = v_0(T, w_0) \tag{4}$$

where the dependence of u_0 and v_0 on w_0 is intrinsically nonlinear as it describes the mid-plane stretching, a nonlinear effect of the transverse motions.

The next group of terms present in the in-plane displacements consists of $z\dfrac{\partial w_0(x,y,t)}{\partial x}$ and $z\dfrac{\partial w_0(x,y,t)}{\partial y}$ which readily are recognized as the first order plate bending components and are linear in the plate transverse coordinate. Completing the formulation of $u(x,y,t)$ and $v(x,y,t)$ are the terms $z\left[1-\dfrac{4}{3}\left(\dfrac{z}{h}\right)^2\right]\varphi_u(x,y,t)$, and $z\left[1-\dfrac{4}{3}\left(\dfrac{z}{h}\right)^2\right]\varphi_v(x,y,t)$ which represent the higher order plate bending corrections. Generally speaking, these components take the form $g(z)\varphi(x,y,t)$ and are designed to account for a nonlinear distribution of the displacements across the thickness. The selection of the function $H(z)$, $H(z)=z\left[1-\dfrac{4}{3}\left(\dfrac{z}{h}\right)^2\right]$, and the physical interpretation of the functions $\varphi_u(x,y,t)$ and $\varphi_v(x,y,t)$ will be discussed in the next section in connection with the strains. Clearly, these terms are primarily produced by the transverse motions and thus

$$\varphi_u = \varphi_u(w_0) \qquad \text{and} \qquad \varphi_v = \varphi_v(w_0)\ . \tag{5}$$

It will be shown, under the assumption of a symmetric composite layering, that φ_u and φ_v exhibit a linear functional dependence with respect to w_0.

Considering finally the transverse displacement, it is seen that the variations of this quantity across the thickness have been neglected in accordance with (reasonably) thin plate assumptions. Then, $w_0(x,y,t)$ denotes the time-dependent transverse displacement of the mid-plane, produced by external loading and influenced by the in-plane (membrane) stresses as described earlier.

The next step in the structural dynamic modeling of the panel is the introduction of the strains-displacements relationships. The presence of an in-plane displacement field of order $(w_0)^0$, i.e. the one corresponding to the thermal effects only, requires the consideration, even for the small amplitude transverse vibration problem, of nonlinear terms in the definition of the strains. In the present analysis, it will be assumed that the in-plane displacements are substantially smaller than their transverse counterparts so that the second order terms in u and v are neglected but those in w are retained. This approach yields the von Karman strains

$$\varepsilon_x = \frac{\partial u}{\partial x} + \frac{1}{2}\left(\frac{\partial w}{\partial x}\right)^2 \qquad \varepsilon_y = \frac{\partial v}{\partial y} + \frac{1}{2}\left(\frac{\partial w}{\partial y}\right)^2 \qquad \varepsilon_z = \frac{\partial w}{\partial z} = 0$$

(6)

$$\gamma_{xy} = \frac{1}{2}\left[\frac{\partial u}{\partial y} + \frac{\partial v}{\partial x} + \left(\frac{\partial w}{\partial x}\right)\left(\frac{\partial w}{\partial y}\right)\right] \qquad \gamma_{xz} = \frac{1}{2}\left[\frac{\partial u}{\partial z} + \frac{\partial w}{\partial x}\right] \qquad \gamma_{yz} = \frac{1}{2}\left[\frac{\partial v}{\partial z} + \frac{\partial w}{\partial y}\right].$$

Introducing the displacement field given by Eq. (1)-(3) in Eq. (6) yields the expressions of the strains in terms of the five basic unknowns, i.e. $u_0(x, y, t)$, $v_0(x, y, t)$, $w_0(x, y, t)$, $\varphi_u(x, y, t)$, and $\varphi_v(x, y, t)$. In this respect, note at the contrary of first order bending theory, that the shears strains γ_{xz} and γ_{yz} do not vanish inside the plate. In fact, one has

$$\gamma_{xz} = \frac{1}{2}\left[1 - 4\left(\frac{z}{h}\right)^2\right]\varphi_u(x, y, t) \quad \text{and} \quad \gamma_{yz} = \frac{1}{2}\left[1 - 4\left(\frac{z}{h}\right)^2\right]\varphi_v(x, y, t) \qquad (7)$$

from which it is then seen that the function $g(z)$ was selected so that the shear strains γ_{xz} and γ_{yz} vanish at both the top and the bottom of the plate ($z = \pm\frac{h}{2}$) as required by the no shear stress boundary conditions. Further, Eq. (7) implies that $\varphi_u(x, y, t)$ and $\varphi_v(x, y, t)$ are in fact directly related to the mid-plane ($z = 0$) shears γ_{xz} and γ_{yz}. The higher order plate bending displacement field given by Eq. (1)-(3) thus includes shear effects.

Turning now to the definition of the stresses, it will be assumed that the behavior of the panel remains linearly elastic during its entire fatigue life. Modeling further each layer of the composite as an orthotropic material leads to the stress-strain relationships

$$\underline{\sigma}' = \begin{Bmatrix} \sigma_{x'} \\ \sigma_{y'} \\ \sigma_z \\ \tau_{x'z} \\ \tau_{y'z} \\ \tau_{x'y'} \end{Bmatrix} = Q \begin{Bmatrix} \varepsilon_{x'} - \alpha_{x'} T \\ \varepsilon_{y'} - \alpha_{y'} T \\ \varepsilon_z \\ \varepsilon_{x'z} \\ \varepsilon_{y'z} \\ \varepsilon_{x'y'} \end{Bmatrix} = Q\,\underline{\varepsilon}' - Q\,\underline{\alpha}'\,T \qquad (8)$$

where (x', y', z) denotes the frame of reference for each layer with x' aligned with the fibers. Further, $\alpha_{x'}$ and $\alpha_{y'}$ represent the coefficients of thermal expansion along and across fibers and $T = T(x, y, z)$ is the local temperature. Finally, $\varepsilon_{x'y'} = 2\gamma_{x'y'}$, $\varepsilon_{x'z} = 2\gamma_{x'z}$, and similarly $\varepsilon_{y'z} = 2\gamma_{y'z}$, and Q denotes the symmetric elastic constant matrix of the orthotropic layer, i.e.,

$$Q = \begin{bmatrix} Q_{11} & Q_{12} & Q_{13} & 0 & 0 & 0 \\ Q_{12} & Q_{22} & Q_{23} & 0 & 0 & 0 \\ Q_{13} & Q_{23} & Q_{33} & 0 & 0 & 0 \\ 0 & 0 & 0 & Q_{44} & 0 & 0 \\ 0 & 0 & 0 & 0 & Q_{55} & 0 \\ 0 & 0 & 0 & 0 & 0 & Q_{66} \end{bmatrix}. \tag{9}$$

Since the strains are defined in the global axes (x, y, z), see Eq. (6), it is necessary to rewrite Eq. (8) in that frame of reference. Specifically, it is found that

$$\underline{\sigma} = R(\phi_k)\,\underline{\sigma}' = R(\phi_k)\,Q\,R(-\phi_k)\,\underline{\varepsilon} - R(\phi_k)\,Q\,\underline{\alpha}'\,T \tag{10}$$

where $R(\phi_k)$ denotes the 6x6 matrix describing the rotation from (x', y', z) to (x, y, z) by the ply angle ϕ_k. That is,

$$R(\phi_k) = \begin{bmatrix} m^2 & n^2 & 0 & -2mn & 0 & 0 \\ n^2 & m^2 & 0 & 2mn & 0 & 0 \\ 0 & 0 & 1 & 0 & 0 & 0 \\ mn & -mn & 0 & m^2 - n^2 & 0 & 0 \\ 0 & 0 & 0 & 0 & m & -n \\ 0 & 0 & 0 & 0 & n & m \end{bmatrix} \tag{11}$$

where $m = \cos\phi_k$ and $n = \sin\phi_k$. For simplicity of notation, Eq. (10) will be rewritten as

$$\underline{\sigma} = \overline{Q}\left[\underline{\varepsilon} - \underline{\alpha}\,T\right] \tag{12}$$

where

$$\overline{Q} = R(\phi_k)\,Q\,R(-\phi_k) \qquad \text{and} \qquad \underline{\alpha}\,T = \left[R(-\phi_k)\right]^{-1}\underline{\alpha}'\,T = R(\phi_k)\,\underline{\alpha}'\,T \tag{13}$$

Equations (1)-(3), (6), and (8)-(13) provide a complete description of the displacement, strain, and stress fields in terms of the functions $u_0(x, y, t)$, $v_0(x, y, t)$, $w_0(x, y, t)$, $\varphi_u(x, y, t)$, and $\varphi_v(x, y, t)$. Then, to obtain the set of governing equations for these unknowns, Hamilton's principle can be used, i.e.

$$\delta \int_{t_1}^{t_2} \left(T - V + W_{ext}\right) dt = 0 \tag{14}$$

where T, V, and W_{ext} denote respectively the kinetic and potential energies and the work done by the external (acoustic) loading. These quantities are readily obtained from the displacement, strain, and stress fields as

$$T = \frac{1}{2}\int_0^a \int_0^b \int_{-h/2}^{h/2} \rho\left(\dot{u}^2 + \dot{v}^2 + \dot{w}^2\right) dz\, dy\, dx \tag{15}$$

$$V = \frac{1}{2}\int_0^a \int_0^b \left[\sum_{k=1}^{n_p} \int_{z_k}^{z_{k+1}} \underline{\sigma}^T\left[\underline{\varepsilon} - \underline{\alpha}\,T\right] dz\right] dy\, dx \tag{16}$$

where n_p represents the number of plies and z_k, z_{k+1} are the transverse coordinates of the bottom and top of the k^{th} ply. Finally, the external work is defined by its virtual counterpart

$$\delta W_{ext} = \int_0^a \int_0^b p(x, y, t)\, \delta w \, dy \, dx \tag{17}$$

where $p(x, y, t)$ denotes the acoustic pressure exerted on the surface of the panel.

The application of Hamilton's principle, Eq. (14), to the above quantities yields a set of five nonlinear coupled partial differential equations for the quantities $u_0(x, y, t)$, $v_0(x, y, t)$, $w_0(x, y, t)$, $\varphi_u(x, y, t)$, and $\varphi_v(x, y, t)$ the solution of which represents a serious challenge even in the case of a deterministic loading $p(x, y, t)$. In the presence of random acoustic pressure fluctuations, the determination of the statistical description, e.g. probability density functions, of the five variables is beyond current capabilities and a simplification of the model must be achieved.

2.2 Derivation of Simplified Models

Several methods are available for the derivation of simplified models for nonlinear structural dynamic problems. One standard approach is to proceed as for linear systems and express the unknown displacements fields in a limited modal-type expansion. In the present context, this strategy would lead to the approximation

$$\underline{Z} = \sum_{i=1}^{m} q_i(t)\, \underline{\psi}(x, y) \tag{18}$$

where

$$\underline{Z}^T = [u_0(x, y, t), v_0(x, y, t), w_0(x, y, t), \varphi_u(x, y, t), \varphi_v(x, y, t)] \tag{19}$$

and $\underline{\psi}(x, y)$ denotes a five-component vector of specified functions of the spatial coordinates x and y. Finally, the time-dependence of the displacement fields is captured by the unknown variables $q_i(t)$. When the governing equations for $\underline{Z}$ are linear or weakly nonlinear, the number of modes m can be selected to be substantially smaller than the dimension of the vector $\underline{Z}$ and a sometime dramatic simplification of the problem is accomplished. A single-mode (m=1) approximation is especially attractive as it reduces the problem to a single, nonlinear, ordinary differential equation. Unfortunately, in this low order approximation the components of the vector $\underline{Z}$ are *linearly* dependent on each other which is not acceptable in the present context since the in-plane displacements $u_0(x, y, t)$ and $v_0(x, y, t)$ involve the transverse deflections $w_0(x, y, t)$ only through the mid-plane stretching, a purely nonlinear effect.

The derivation of a single-mode approximation of the present problem must then be accomplished differently. Specifically, it was already argued in connection with the selection of the von Karman strains that the in-plane displacements are expected to be substantially smaller than their transverse counterparts. Thus, the contribution to the panel kinetic energy of the terms $\dot{u}^2$ and $\dot{v}^2$ should be small and could, in first approximation, be neglected. Accordingly, the displacement fields $u_0(x, y, t)$, $v_0(x, y, t)$,

$\varphi_u(x, y, t)$, and $\varphi_v(x, y, t)$ appear explicitly only in the potential energy and must then be selected so that $\delta V = 0$. Note that the potential energy does not involve any time derivatives so that its minimization with respect to $u_0(x, y, t)$, $v_0(x, y, t)$, $\varphi_u(x, y, t)$, and $\varphi_v(x, y, t)$ yields a set of four nonlinear, coupled partial differential equations with respect to space for these four displacement fields. These equations can be recognized as integral versions of the in-plane equilibrium condition for the plate and can be used to express (at least approximately) $u_0(x, y, t)$, $v_0(x, y, t)$, $\varphi_u(x, y, t)$, and $\varphi_v(x, y, t)$ in terms of the transverse deflection $w_0(x, y, t)$. Practically speaking, this procedure represents a quasi-static condensation of the plate equations and leads to the single unknown field $w_0(x, y, t)$ which, following previous arguments (see Eq. (16)-(17)), can be sought in the form

$$w_0(x, y, t) = q(t)\,\overline{w}_0(x, y) \tag{20}$$

where $\overline{w}_0(x, y)$ is a specified function. For maximum accuracy, $\overline{w}_0(x, y)$ should closely resemble the spatial distribution of the plate transverse deflections and thus can be selected as the panel buckling mode shape. Mathematically, this function can be expressed as

$$\overline{w}_0(x, y) = \sum_m \sum_n a_{mn} \sin\left(\frac{m\pi x}{a}\right) \sin\left(\frac{n\pi y}{b}\right) \tag{21}$$

where a and b are the dimensions of the plate in the x and y directions, respectively.

At this point of the investigation, it is assumed that the panel is simply supported and thus the function $\overline{w}_0(x, y)$ should satisfy zero deflection boundary conditions on its four sides, i.e. on $x = 0$, $x = a$, $y = 0$, and $y = b$. These conditions are automatically fulfilled by the choice of the sine functions independently of the number of terms in the summation. Thus, for simplicity, it will be assumed that

$$\overline{w}_0(x, y) = \sin\left(\frac{m\pi x}{a}\right) \sin\left(\frac{n\pi y}{b}\right). \tag{22}$$

The above discussion demonstrates that the determination of a single-mode approximation of the panel dynamic behavior can be separated in the following two steps:

(1) Determination of the functional dependence of $u_0(x, y, t)$, $v_0(x, y, t)$, $\varphi_u(x, y, t)$, and $\varphi_v(x, y, t)$ on $w_0(x, y, t)$

(2) Determination of the governing equation for the transverse displacement, i.e. $q(t)$.

Before addressing each of these two aspects of the problem, the following notations are first introduced:

Forces:

$$N_\gamma = \int_{-h/2}^{h/2} \sigma_\gamma \, dz \qquad M_\gamma = \int_{-h/2}^{h/2} z\,\sigma_\gamma \, dz \qquad P_\gamma = \int_{-h/2}^{h/2} H(z)\,\sigma_\gamma \, dz \qquad \gamma = x, y \tag{23}$$

$$N_{xy} = \int_{-h/2}^{h/2} \tau_{xy} \, dz \qquad M_{xy} = \int_{-h/2}^{h/2} z\,\tau_{xy} \, dz \qquad P_{xy} = \int_{-h/2}^{h/2} H(z)\,\tau_{xy} \, dz \tag{24}$$

$$\underline{N} = \left[N_x \; N_y \; N_{xy}\right]^T \qquad \underline{M} = \left[M_x \; M_y \; M_{xy}\right]^T \qquad \underline{P} = \left[P_x \; P_y \; P_{xy}\right]^T \tag{25}$$

$$R_{xz} = \int_{-h/2}^{h/2} \frac{dH(z)}{dz} \tau_{xz} \, dz \qquad R_{yz} = \int_{-h/2}^{h/2} \frac{dH(z)}{dz} \tau_{yz} \, dz \qquad \underline{R} = \left[R_{xz} \; R_{yz}\right]^T \tag{26}$$

Thermal Loading:

$$\underline{N}^t = \int_{-h/2}^{h/2} \tilde{Q} \, \tilde{\underline{\alpha}} \, T \, dz \qquad \underline{M}^t = \int_{-h/2}^{h/2} z \, \tilde{Q} \, \tilde{\underline{\alpha}} \, T \, dz \qquad \underline{P}^t = \int_{-h/2}^{h/2} H(z) \, \tilde{Q} \, \tilde{\underline{\alpha}} \, T \, dz \tag{27}$$

where $\tilde{Q}$ is the 3x3 matrix extracted from $\overline{Q}$ by removing the 3rd, 4th, and 5th rows and columns and $\tilde{\underline{\alpha}}$ is the 3-component vector corresponding similarly to $\underline{\alpha}$.

Strains/Curvatures:

$$\underline{\varepsilon}^0 = \left[\frac{\partial u_0}{\partial x} + \frac{1}{2}\left(\frac{\partial w_0}{\partial x}\right)^2 \quad \frac{\partial v_0}{\partial y} + \frac{1}{2}\left(\frac{\partial w_0}{\partial y}\right)^2 \quad \frac{\partial u_0}{\partial y} + \frac{\partial v_0}{\partial x} + \left(\frac{\partial w_0}{\partial x}\right)\left(\frac{\partial w_0}{\partial y}\right)\right]^T \tag{28}$$

$$\underline{\kappa} = \left[-\frac{\partial^2 w_0}{\partial x^2} \quad -\frac{\partial^2 w_0}{\partial y^2} \quad -2\frac{\partial^2 w_0}{\partial x \partial y}\right]^T \tag{29}$$

$$\underline{\phi} = \left[\varphi_u \;\; \varphi_v\right]^T \qquad \underline{\phi}' = \left[\frac{\partial \varphi_u}{\partial x} \quad \frac{\partial \varphi_v}{\partial y} \quad \frac{\partial \varphi_u}{\partial y} + \frac{\partial \varphi_v}{\partial x}\right]^T \tag{30}$$

Constitutive Matrices:

$$(A, B, C, R, X, W, Z) = \int_{-h/2}^{h/2} \left(1, z, z^2, \left(\frac{dH(z)}{dz}\right)^2, zH(z), H^2(z), H(z)\right) \overline{Q} \, dz \; . \tag{31}$$

Further, $\tilde{A}$, $\tilde{B}$, $\tilde{C}$, $\tilde{X}$, $\tilde{W}$, and $\tilde{Z}$ are the 3x3 matrices extracted from A, B, C, X, W, and Z, respectively, by removing the 3rd, 4th, and 5th rows and columns and

$$\tilde{R} = \begin{bmatrix} R_{44} & R_{45} \\ R_{45} & R_{55} \end{bmatrix}. \tag{32}$$

Relations between force and strain vectors can be derived by multiplying the constitutive equation, Eq. (12), by 1, z, $H(z)$, and $\frac{dH(z)}{dz}$ and integrating through the panel thickness. Specifically, it is found that

$$\begin{bmatrix} \underline{N} \\ \underline{M} \\ \underline{P} \\ \underline{R} \end{bmatrix} = \begin{bmatrix} \tilde{A} & \tilde{B} & \tilde{Z} & 0 \\ \tilde{B} & \tilde{C} & \tilde{X} & 0 \\ \tilde{Z} & \tilde{X} & \tilde{W} & 0 \\ 0 & 0 & 0 & \tilde{R} \end{bmatrix} \begin{bmatrix} \underline{\varepsilon}^0 \\ \underline{\kappa} \\ \underline{\phi}' \\ \underline{\phi} \end{bmatrix} - \begin{bmatrix} \underline{N}^t \\ \underline{M}^t \\ \underline{P}^t \\ \underline{0} \end{bmatrix}. \tag{33}$$

2.2.1 Determination of the functional dependence of $u_0(x, y, t)$, $v_0(x, y, t)$, $\varphi_u(x, y, t)$, and $\varphi_v(x, y, t)$ on $w_0(x, y, t)$

Proceeding under the assumption that the kinetic energy associated with the displacements/shears $u_0(x, y, t)$, $v_0(x, y, t)$, $\varphi_u(x, y, t)$, and $\varphi_v(x, y, t)$ can be neglected in comparison with its out-of-plane deflection component, the governing equations for these functions derived from Hamilton's principle correspond in fact to the minimization of the potential energy alone. Then, the condition $\delta V = 0$ yields, after some integrations by parts, the 4 partial differential equations

$$\delta u_0 : \qquad \frac{\partial N_x}{\partial x} + \frac{\partial N_{xy}}{\partial y} = 0 \tag{34}$$

$$\delta v_0 : \qquad \frac{\partial N_{xy}}{\partial x} + \frac{\partial N_y}{\partial y} = 0 \tag{35}$$

$$\delta \varphi_u : \qquad \frac{\partial P_x}{\partial x} + \frac{\partial P_{xy}}{\partial y} - R_{xz} = 0 \tag{36}$$

$$\delta \varphi_v : \qquad \frac{\partial P_{xy}}{\partial x} + \frac{\partial P_y}{\partial y} - R_{yz} = 0 . \tag{37}$$

In order to obtain closed form expressions for the displacements/shears $u_0(x, y, t)$, $v_0(x, y, t)$, $\varphi_u(x, y, t)$, and $\varphi_v(x, y, t)$, it is necessary to specify the temperature distribution in the plate. Following Lee (1993), it will be assumed here that

$$T = T_0 + \delta_v \, T_0 \sin\frac{\pi x}{a} \sin\frac{\pi y}{b} + \delta_g \, T_0 \left[\sin^2\frac{\pi x}{a} \sin^2\frac{\pi y}{b} - \frac{1}{4} \right] \frac{z}{h} \tag{38}$$

where T_0 denotes the average plate temperature and δ_v and δ_g represent measures of the temperature gradient along and across the plate, respectively. Then, introduce the vectors

$$\underline{\nu} = \int_{-h/2}^{h/2} \tilde{Q}\, \underline{\tilde{\alpha}} \, dz \qquad \underline{\psi} = \int_{-h/2}^{h/2} z\, \tilde{Q}\, \underline{\tilde{\alpha}} \, dz \qquad \underline{\theta} = \frac{1}{h} \int_{-h/2}^{h/2} z^2\, \tilde{Q}\, \underline{\tilde{\alpha}} \, dz$$

$$\underline{\chi} = \int_{-h/2}^{h/2} H(z)\, \tilde{Q}\, \underline{\tilde{\alpha}} \, dz \qquad \underline{\mu} = \frac{1}{h} \int_{-h/2}^{h/2} z\, H(z)\, \tilde{Q}\, \underline{\tilde{\alpha}} \, dz . \tag{39}$$

Under these assumptions, it is found that

$$\underline{N}^t = \left[T_0 + \delta_v \, T_0 \sin\frac{\pi x}{a} \sin\frac{\pi y}{b} \right] \underline{\nu} + \frac{1}{h} \delta_g \, T_0 \left[\sin^2\frac{\pi x}{a} \sin^2\frac{\pi y}{b} - \frac{1}{4} \right] \underline{\psi} \tag{40}$$

$$\underline{M}^t = \left[T_0 + \delta_v\, T_0 \sin\frac{\pi x}{a}\sin\frac{\pi y}{b}\right]\underline{\psi} + \delta_g\, T_0\left[\sin^2\frac{\pi x}{a}\sin^2\frac{\pi y}{b} - \frac{1}{4}\right]\underline{\theta} \tag{41}$$

and

$$\underline{P}^t = \left[T_0 + \delta_v\, T_0 \sin\frac{\pi x}{a}\sin\frac{\pi y}{b}\right]\underline{\chi} + \delta_g\, T_0\left[\sin^2\frac{\pi x}{a}\sin^2\frac{\pi y}{b} - \frac{1}{4}\right]\underline{\mu} \tag{42}$$

Next, it will be assumed, as is often the case, that the panel is composed of symmetrically placed layers. Then, it is readily seen that the matrices B, Z, $\widetilde{B}$, $\widetilde{Z}$, and vectors $\underline{\psi}$ and $\underline{\chi}$ are identically zero and the in-plane displacements $u_0(x, y, t)$, $v_0(x, y, t)$ and out-of-plane shears $\varphi_u(x, y, t)$, and $\varphi_v(x, y, t)$ are uncoupled of each other, see Eq. (33)-(37). The determination of these two sets of functions can thus be accomplished separately as follows.

(a) Determination of the in-plane displacements $u_0(x, y, t)$, $v_0(x, y, t)$

The determination of the in-plane displacements $u_0(x, y, t)$, $v_0(x, y, t)$ is accomplished from Eq. (34)-(35) and the reduced constitutive relation Eq. (33), i.e.

$$\underline{N} = \widetilde{A}\,\underline{\varepsilon}^0 - \underline{N}^t, \tag{43}$$

in either of two ways. A first approach is to introduce this expression for the force vector $\underline{N}$ in Eq. (34) and (35) to obtain two coupled partial differential equations for $u_0(x, y, t)$, $v_0(x, y, t)$ (no time derivatives). Another strategy is to introduce a scalar stress function $\hat{\psi}(x, y, t)$ such that (see Lee et al., 1998 for details)

$$N_x = \frac{\partial^2\hat{\psi}}{\partial y^2} \qquad N_y = \frac{\partial^2\hat{\psi}}{\partial x^2} \qquad N_{xy} = -\frac{\partial^2\hat{\psi}}{\partial x\partial y} \tag{44}$$

so that the equilibrium equations (34) and (35) are automatically satisfied. Then, the function $\hat{\psi}(x, y, t)$ is selected to satisfy the compatibility condition

$$\frac{\partial^2\varepsilon_1^0}{\partial y^2} + \frac{\partial^2\varepsilon_2^0}{\partial x^2} - \frac{\partial^2\varepsilon_3^0}{\partial x\partial y} = \left(\frac{\partial^2 w}{\partial x\partial y}\right)^2 - \left(\frac{\partial^2 w}{\partial x^2}\right)\left(\frac{\partial^2 w}{\partial y^2}\right) \tag{45}$$

where ε_1^0, ε_2^0, and ε_3^0 are the components of the vector $\underline{\varepsilon}^0$, see Eq. (28), which are related to $\hat{\psi}(x, y, t)$ through Eq. (43) and (44). This process results in the 4th order partial differential equation for $\hat{\psi}(x, y, t)$ presented by Lee et al. (1998).

Irrespectively of the approach selected, it is necessary to first establish the boundary conditions to be satisfied. In view of the simply supported nature of the plate, it could be expected that the in-plane motions of the mid-plane be restricted at the support, i.e.

$$u(0, y, t) = u(a, y, t) = u(x, 0, t) = u(x, b, t) = v(0, y, t) = v(a, y, t) = v(x, 0, t) = v(x, b, t) = 0 \tag{46}$$

Of these 8 boundary conditions, it is particularly important that

$$u(0, y, t) = u(a, y, t) = v(x, 0, t) = v(x, b, t) = 0 \tag{47}$$

be satisfied as they correspond to the constraint on the expansion of the plate and thus play a fundamental role in the buckling of the plate. The remaining four geometric boundary conditions

$$u(x, 0, t) = u(x, b, t) = v(0, y, t) = v(a, y, t) = 0 \tag{48}$$

represent a lack of sliding along the supports. If necessary for simplicity, they could be replaced by their corresponding natural boundary conditions

$$\tau_{xy}(x, 0, t) = \tau_{xy}(x, b, t) = \tau_{xy}(0, y, t) = \tau_{xy}(a, y, t) = 0 \tag{49}$$

on the midplane, $z = 0$.

The determination of closed form solutions of nonhomogenous partial differential equations, such as those for $u_0(x, y, t)$ and $v_0(x, y, t)$ or $\hat{\psi}(x, y, t)$, is conditional on the availability of both particular and homogenous solutions. Considering first the former, it is seen that the nonhomogenous character of these equations originates with both the transverse displacement $w_0(x, y, t)$ and the in-plane temperature variation both of which involve trigonometric functions of *x/a* and *y/b*. On this basis, a particular solution can be sought as a limited Fourier series. On the other hand, the determination of a homogenous solution which, after superposition with its particular counterpart, yields the correct boundary conditions is in general a daunting task unless the method of separation of variables can be used. In this light, it should be noted that

(i) the Fourier series particular solution for $u_0(x, y, t)$ and $v_0(x, y, t)$ does not satisfy any of the boundary conditions given by Eq. (46) and/or (49) when A_{16} and A_{26} do not vanish.

(ii) the partial differential equations to be solved do not admit a separation of variables homogenous solution when A_{16} and A_{26} do not vanish.

It is then concluded that a closed form solution for the in-plane displacements $u_0(x, y, t)$ and $v_0(x, y, t)$ will be quite difficult to obtain when the two coefficients A_{16} and A_{26} are non-zero. For this reason, the present analysis will be limited to either symmetric angle-ply laminates or cross-ply laminates in both of which the constants A_{16} and A_{26} always vanish. Under this restriction, a bonafide solution, satisfying Eq. (47) and (49), can be found as

$$u_0(x, y, t) = u_{01} \sin\frac{2\pi x}{a} + u_{02} \sin\frac{2\pi x}{a} \cos\frac{2\pi y}{b} \tag{50}$$

$$v_0(x, y, t) = v_{01} \sin\frac{2\pi y}{b} + v_{02} \cos\frac{2\pi x}{a} \sin\frac{2\pi y}{b} \tag{51}$$

$$\begin{aligned} N_x(x, y, t) = C_{60}\, q^2 - \nu_1 T_0 - \frac{4\pi^2}{b^2}\left(\lambda_{020}\, q^2 + \lambda_{021}\, \delta_v T_0\right)\cos\frac{2\pi y}{b} \\ - \frac{4\pi^2}{b^2}\lambda_{221}\, \delta_v T_0 \cos\frac{2\pi x}{a} \cos\frac{2\pi y}{b} \end{aligned} \tag{52}$$

$$N_y(x,y,t) = C_{50}\, q^2 - \nu_2\, T_0 - \frac{4\pi^2}{a^2}\left(\lambda_{200}\, q^2 + \lambda_{201}\, \delta_v\, T_0\right)\cos\frac{2\pi x}{a} - \frac{4\pi^2}{a^2}\,\lambda_{221}\,\delta_v\, T_0 \cos\frac{2\pi x}{a}\,\cos\frac{2\pi y}{b} \tag{53}$$

$$N_{xy}(x,y,t) = -\frac{4\pi^2}{ab}\,\lambda_{221}\,\delta_v\, T_0 \sin\frac{2\pi x}{a}\,\sin\frac{2\pi y}{b} \tag{54}$$

where

$$C_{50} = \frac{\pi^2}{8a^2b^2}\left[A_{22}\,a^2 + A_{12}\,b^2\right] \qquad C_{60} = \frac{\pi^2}{8a^2b^2}\left[A_{12}\,a^2 + A_{11}\,b^2\right] \tag{55}$$

$$\lambda_{200} = \frac{a^2}{32b^2}\,\frac{A_{11}\,A_{22} - A_{12}^2}{A_{11}} \qquad \lambda_{201} = -\frac{a^2}{16\pi^2}\,\frac{(\nu_2\,A_{11} - \nu_1\,A_{12})}{A_{11}} \tag{56}$$

$$\lambda_{020} = \frac{b^2}{32a^2}\,\frac{A_{11}\,A_{22} - A_{12}^2}{A_{22}} \qquad \lambda_{201} = -\frac{b^2}{16\pi^2}\,\frac{(\nu_1\,A_{22} - \nu_2\,A_{12})}{A_{22}} \tag{57}$$

$$\lambda_{221} = \frac{1}{16\pi^2}\,\frac{\nu_1\left(\frac{A_{22}}{b^2} - \frac{A_{12}}{a^2}\right) + \nu_2\left(\frac{A_{11}}{a^2} - \frac{A_{12}}{b^2}\right)}{\frac{A_{11}}{a^4} + \frac{(\Lambda - 2A_{12})}{a^2b^2} + \frac{A_{22}}{b^4}} \qquad \Lambda = \frac{A_{11}\,A_{22}\,A_{12}^2}{A_{66}} \tag{58}$$

$$u_{01} = -q^2\,\frac{2\pi}{a}\left(\frac{1}{16} - \frac{\lambda_{200}\,A_{12}}{A_{11}\,A_{22} - A_{12}^2}\right) - \frac{1}{8\pi a}\,\frac{a^2A_{22}\,\nu_1 - a^2A_{12}\,\nu_2 - 16\pi^2\,\lambda_{201}\,A_{12}}{A_{11}\,A_{22} - A_{12}^2}\,\delta_v\,T_0 \tag{59}$$

$$u_{02} = \frac{\pi}{16a}\,q^2 + \frac{a}{2\pi}\,\frac{1}{A_{11}\,A_{22} - A_{12}^2}\left[\frac{1}{4}\left(A_{22}\,\nu_1 - A_{12}\,\nu_2\right) - \lambda_{221}\left(\frac{4\pi^2}{b^2}\,A_{22} - \frac{4\pi^2}{a^2}\,A_{12}\right)\right]\delta_v\,T_0 \tag{60}$$

$$v_{01} = -q^2\,\frac{2\pi}{b}\left(\frac{1}{16} - \frac{\lambda_{020}\,A_{12}}{A_{11}\,A_{22} - A_{12}^2}\right) - \frac{1}{8\pi b}\,\frac{b^2A_{11}\,\nu_2 - b^2A_{12}\,\nu_1 - 16\pi^2\,\lambda_{021}\,A_{12}}{A_{11}\,A_{22} - A_{12}^2}\,\delta_v\,T_0 \tag{61}$$

$$v_{02} = \frac{\pi}{16b}\,q^2 + \frac{b}{2\pi}\,\frac{1}{A_{11}\,A_{22} - A_{12}^2}\left[\frac{1}{4}\left(A_{11}\,\nu_2 - A_{12}\,\nu_1\right) - \lambda_{221}\left(\frac{4\pi^2}{a^2}\,A_{11} - \frac{4\pi^2}{b^2}\,A_{12}\right)\right]\delta_v\,T_0 \tag{62}$$

(b) Determination of the out-of-plane shears $\varphi_u(x, y, t)$ *and* $\varphi_v(x, y, t)$

A set of two partial differential equations for the out-of-plane shears $\varphi_u(x, y, t)$ and $\varphi_v(x, y, t)$ can be derived from the simplified constitutive equation, Eq. (33), i.e.

$$\begin{bmatrix} \underline{M} \\ \underline{P} \\ \underline{R} \end{bmatrix} = \begin{bmatrix} \widetilde{C} & \widetilde{X} & 0 \\ \widetilde{X} & \widetilde{W} & 0 \\ 0 & 0 & \widetilde{R} \end{bmatrix} \begin{bmatrix} \underline{\kappa} \\ \underline{\phi}' \\ \underline{\phi} \end{bmatrix} - \begin{bmatrix} \underline{M}^t \\ \underline{P}^t \\ 0 \end{bmatrix}, \tag{63}$$

and Eq. (36) and (37). An analysis of their nonhomogenous terms motivates the search for a particular solution of the form

$$\varphi_u(x, y, t) = U_{sc} \sin\frac{\pi x}{a}\cos\frac{\pi y}{b} + U_{cs} \cos\frac{\pi x}{a}\sin\frac{\pi y}{b} \tag{64}$$

$$\varphi_v(x, y, t) = V_{sc} \sin\frac{\pi x}{a}\cos\frac{\pi y}{b} + V_{cs} \cos\frac{\pi x}{a}\sin\frac{\pi y}{b}. \tag{65}$$

Accordingly, the vectors $\underline{P}$, $\underline{\phi}'$, and $\underline{R}$ can be expressed as

$$\underline{P}(x, y, t) = \underline{P}_{ss} \sin\frac{\pi x}{a}\sin\frac{\pi y}{b} + \underline{P}_{cc} \cos\frac{\pi x}{a}\cos\frac{\pi y}{b} \tag{66}$$

$$\underline{\phi}'(x, y, t) = \underline{\phi}'_{ss} \sin\frac{\pi x}{a}\sin\frac{\pi y}{b} + \underline{\phi}'_{cc} \cos\frac{\pi x}{a}\cos\frac{\pi y}{b} \tag{67}$$

$$\underline{R}(x, y, t) = \underline{R}_{sc} \sin\frac{\pi x}{a}\cos\frac{\pi y}{b} + \underline{R}_{cs} \cos\frac{\pi x}{a}\sin\frac{\pi y}{b}. \tag{68}$$

Introducing the partitioned vector $\underline{R}_p = \left[\underline{R}_{cs}^T \; \underline{R}_{sc}^T\right]^T$, it can be seen that Eq. (36) and (37) are equivalent to

$$\Delta_{ss}\, \underline{P}_{ss} + \Delta_{cc}\, \underline{P}_{cc} - \underline{R}_p = \underline{0} \tag{69}$$

where

$$\Delta_{ss} = \begin{bmatrix} \pi/a & 0 & 0 \\ 0 & 0 & \pi/a \\ 0 & 0 & \pi/b \\ 0 & \pi/b & 0 \end{bmatrix} \quad \text{and} \quad \Delta_{cc} = \begin{bmatrix} 0 & 0 & -\pi/b \\ 0 & -\pi/b & 0 \\ -\pi/a & 0 & 0 \\ 0 & 0 & -\pi/a \end{bmatrix}. \tag{70}$$

Further, the constitutive relation, Eq. (63), is equivalent to the equations

$$\underline{P}_{ss} = q\,\widetilde{X}\,\underline{\kappa}_{ss} + \widetilde{W}\,\underline{\phi}'_{ss} - \delta_g\, T_0\, \underline{\mu} \tag{71}$$

$$\underline{P}_{cc} = q\,\widetilde{X}\,\underline{\kappa}_{cc} + \widetilde{W}\,\underline{\phi}'_{cc} \tag{72}$$

where

$$\underline{\kappa}_{ss} = \left[\frac{\pi^2}{a^2} \; \frac{\pi^2}{b^2} \; 0\right]^T \quad \text{and} \quad \underline{\kappa}_{ss} = \left[0 \; 0 \; -\frac{2\pi^2}{ab}\right]^T. \tag{73}$$

Moreover, from the definition of $\underline{\phi}'$, Eq. (30), it is found that

$$\underline{\phi}'_{ss} = -\Delta_{ss}^T \underline{R}_p \qquad \underline{\phi}'_{cc} = -\Delta_{cc}^T \underline{R}_p . \tag{74}$$

Then, combining Eq. (69), (71), (72), and (74) yields the system of algebraic equations

$$\left[\Delta_{ss} \widetilde{W} \Delta_{ss}^T + \Delta_{cc} \widetilde{W} \Delta_{cc}^T + \widetilde{R}_2\right] \underline{R}_p = q\left[\Delta_{ss} \widetilde{X} \underline{\kappa}_{ss} + \Delta_{cc} \widetilde{X} \underline{\kappa}_{cc}\right] - \delta_g T_0 \Delta_{ss} \underline{\mu} \tag{75}$$

with

$$\widetilde{R}_2 = \begin{bmatrix} \widetilde{R} & 0 \\ 0 & \widetilde{R} \end{bmatrix} . \tag{76}$$

Once the coefficients U_{sc}, U_{cs}, V_{sc}, and V_{cs}, stacked in the vector $\underline{R}_p$ have been determined from Eq. (75), the particular solution for the out-of-plane shears $\varphi_u(x, y, t)$, and $\varphi_v(x, y, t)$ is available from Eq. (64) and (65). Further, the corresponding moments can be evaluated from Eq. (63) as

$$\underline{M}(x, y, t) = \underline{M}_{ss} \sin\frac{\pi x}{a} \sin\frac{\pi y}{b} + \underline{M}_{cc} \cos\frac{\pi x}{a} \cos\frac{\pi y}{b} \tag{77}$$

where

$$\underline{M}_{ss} = q \widetilde{C} \underline{\kappa}_{ss} + \widetilde{X} \underline{\phi}'_{ss} - \delta_g T_0 \underline{\theta} = q \widetilde{C} \underline{\kappa}_{ss} - \widetilde{X} \Delta_{ss}^T \underline{R}_p - \delta_g T_0 \underline{\theta} \tag{78}$$

$$\underline{M}_{cc} = q \widetilde{C} \underline{\kappa}_{cc} + \widetilde{X} \underline{\phi}'_{cc} = q \widetilde{C} \underline{\kappa}_{cc} - \widetilde{X} \Delta_{cc}^T \underline{R}_p . \tag{79}$$

The above derivations focused on the particular solution for the out-of-plane shears $\varphi_u(x, y, t)$, and $\varphi_v(x, y, t)$. To complete the solution, it remains to assess the boundary conditions and to determine a corresponding homogenous solution for these functions. Considering first the boundary conditions, it is readily seen that they do not come from the in-plane considerations since the contributions of $\varphi_u(x, y, t)$ and $\varphi_v(x, y, t)$ to the displacements and strains vanish on the mid-plane ($z = 0$) where the in-plane constraints are imposed. Rather, the necessary boundary conditions must come from:

(i) the variational formulation, i.e. $\delta V = 0$

(ii) transverse motion requirements.

In addition to Eq. (36) and (37), the minimization of the potential energy yielded two boundary terms which should also vanish. This situation occurs when:

either φ_u is fixed or $P_x = 0$ and either φ_v is fixed or $P_{xy} = 0$ on $x = 0$ and a (80)

and

either φ_u is fixed or $P_{xy} = 0$ and either φ_v is fixed or $P_y = 0$ on $y = 0$ and b . (81)

Further, the simply supported nature of the plate implies that the moments at the supports should vanish, that is

$$M_x = 0 \qquad \text{on } x = 0 \text{ and } a \tag{82}$$

and

$$M_y = 0 \qquad \text{on } y = 0 \text{ and } b . \tag{83}$$

It is clearly seen from Eq. (64)-(66) and (77) that none of the boundary conditions (80)-(83) is pointwise satisfied by the particular solution derived above and thus it should be necessary to determine an appropriate homogenous solution. The discussion conducted in

connection with the homogenous part of the in-plane problem can be repeated here to demonstrate that such a solution is very unlikely to admit a closed form expression. A first strategy to resolve this issue is to restrict the current analysis, as in the in-plane problem, to plate configurations in which boundary conditions are satisfied exactly by the particular solution presented above. This situation occurs if the terms X_{16} and X_{26} vanish, as is the case in cross-ply laminates. Indeed, it is then found that $U_{sc} = V_{cs} = 0$ so that

$$P_x = 0 \qquad \varphi_v = 0 \qquad M_x = 0 \qquad \text{on } x = 0 \text{ and } a \tag{84}$$

$$P_y = 0 \qquad \varphi_u = 0 \qquad M_y = 0 \qquad \text{on } y = 0 \text{ and } b. \tag{85}$$

In considering the boundary conditions, it should be noted that the imposition of $\varphi_v = 0$ and/or $\varphi_u = 0$ at the plate supports does not imply that the in-plane displacements will vanish there since the terms $z\dfrac{\partial w_0}{\partial x}$ and $z\dfrac{\partial w_0}{\partial y}$ are in general non-zero. Thus, it is unclear that constraining the values of φ_u and φ_v at the edges of the plate would be representative of a typical simple support configuration. Rather, it would appears that the most physical boundary conditions for the present problem would be

$$P_x = 0 \qquad P_{xy} = 0 \qquad M_x = 0 \qquad \text{on } x = 0 \text{ and } a \tag{86}$$

$$P_y = 0 \qquad P_{xy} = 0 \qquad M_y = 0 \qquad \text{on } y = 0 \text{ and } b. \tag{87}$$

Further, note that the above constraints are all *natural* boundary conditions, i.e. they are not related to the geometry of the problem but rather arise through the variational formulation. Thus, the satisfaction of these conditions is *desired* to obtain the best approximation to the exact solution but it is not absolutely required as were the in-plane constraints, Eq. (47). Finally, note that if Eq. (86) and (87) are not satisfied pointwise, they are matched in average along the sides $x = 0, a$ and $y = 0, b$. On the basis of these comments, it is suggested, as an alternative approach to requiring X_{16} and X_{26} to vanish, to require that the natural boundary conditions be satisfied only on average and to let the variational formulation find the best approximation possible to the transverse response problem.

2.2.2 Determination of the governing equation for the transverse displacement, $q(t)$

The mathematical developments presented in the previous section have demonstrated that the search for a transverse response of the plate as

$$w_0(x, y, t) = q(t)\,\overline{w}_0(x, y) \tag{88}$$

must be accompanied by corresponding approximations of the functions $u_0(x, y, t)$, $v_0(x, y, t)$, $\varphi_u(x, y, t)$, and $\varphi_v(x, y, t)$ of the form

$$u_0(x, y, t) = q^2\,\bar{u}_0(x, y) + \delta_v\, T_0\,\hat{u}_0(x, y) + T_0\,\tilde{u}_0(x, y) \tag{89}$$

$$v_0(x, y, t) = q^2\,\bar{v}_0(x, y) + \delta_v\, T_0\,\hat{v}_0(x, y) + T_0\,\tilde{v}_0(x, y) \tag{90}$$

$$\varphi_u(x, y, t) = q\,\overline{\varphi}_u(x, y) + \delta_g\, T_0\,\hat{\varphi}_u(x, y) \tag{91a}$$

$$\varphi_v(x, y, t) = q\,\overline{\varphi}_v(x, y) + \delta_g\, T_0\,\hat{\varphi}_v(x, y) \tag{91b}$$

where the functions $\bar{u}_0(x,y)$, ..., $\hat{\varphi}_v(x,y)$ are known from the solution of the in-plane problem. Introducing the above expressions in Hamilton's principle, Eq. (14), results, after some algebraic manipulations, in the differential equation

$$M\,\ddot{q} + q\left\{\int_0^a\int_0^b\left[N_x\left(\frac{\partial\bar{w}_0}{\partial x}\right)^2 + N_y\left(\frac{\partial\bar{w}_0}{\partial y}\right)^2 + 2\,N_{xy}\left(\frac{\partial\bar{w}_0}{\partial x}\right)\left(\frac{\partial\bar{w}_0}{\partial y}\right)\right]dy\,dx\right\}$$
$$-\left\{\int_0^a\int_0^b\left[M_x\left(\frac{\partial^2\bar{w}_0}{\partial x^2}\right) + M_y\left(\frac{\partial^2\bar{w}_0}{\partial y^2}\right) + 2\,M_{xy}\left(\frac{\partial^2\bar{w}_0}{\partial x\,\partial y}\right)\right]dy\,dx\right\} - p(t) = 0 \tag{92}$$

where M and $p(t)$ are the modal mass and force, respectively, defined as

$$M = \int_0^a\int_0^b\int_{-h/2}^{h/2}\rho\left[z^2\left(\frac{\partial\bar{w}_0}{\partial x}\right)^2 + z^2\left(\frac{\partial\bar{w}_0}{\partial x}\right)^2 + \bar{w}_0^2\right]dz\,dy\,dx = \frac{ab}{4}\left[1 + \frac{h^2}{12}\left(\frac{\pi^2}{a^2} + \frac{\pi^2}{b^2}\right)\right]\int_{-h/2}^{h/2}\rho\,dz \tag{93}$$

and

$$p(t) = \int_0^a\int_0^b p(x,y,t)\,\bar{w}_0(x,y)\,dy\,dx\,. \tag{94}$$

Note that the expression for the mass given in Eq. (93) includes the effect of the rotary inertia associated with the pure bending rotations $\frac{\partial\bar{w}_0}{\partial x}$ and $\frac{\partial\bar{w}_0}{\partial y}$.

Introducing the expressions for the forces $\underline{N}$ and moments $\underline{M}$ given by Eq. (52)-(54) and (77) in Eq. (92) yields the governing equation for the transverse displacements in the form

$$M\,\ddot{q} + \left(k_0 + k_1\,\delta_v\,T_0 + k_2\,T_0\right)q + \gamma\,q^3 = p_0 + p(t) \tag{95}$$

where

$$k_0 = \frac{ab}{4}\left[\frac{\pi^2}{a^2}M_{xss0} + \frac{\pi^2}{b^2}M_{yss0} - \frac{2\pi^2}{ab}M_{xycc0}\right] \tag{96}$$

$$k_1 = \frac{ab}{4}\left[\frac{2\pi^4}{a^2\,b^2}\left(\lambda_{021} + \lambda_{201}\right) - \frac{\nu_1\,\pi^2}{4a^2} - \frac{\nu_2\,\pi^2}{4b^2}\right] \tag{97}$$

$$k_2 = -\frac{ab}{4}\left[\frac{\nu_1\,\pi^2}{a^2} + \frac{\nu_2\,\pi^2}{b^2}\right] \tag{98}$$

$$\gamma = \frac{ab}{4}\left[\frac{2\pi^4}{a^2\,b^2}\left(\lambda_{020} + \lambda_{200}\right) + \frac{\pi^2\,C_{60}}{a^2} + \frac{\pi^2\,C_{50}}{b^2}\right] \tag{99}$$

$$p_0 = -\frac{ab}{4}\left[\frac{\pi^2}{a^2}M_{xss1} + \frac{\pi^2}{b^2}M_{yss1} - \frac{2\pi^2}{ab}M_{xycc1}\right]\delta_g\,T_0\,. \tag{100}$$

In the above expressions (Eq. (96) and (100)), the symbols M_{xss0} and M_{yss0} are the first two components of the vector $\underline{M}_{ss0}$ which corresponds to the q related terms of $\underline{M}_{ss}$,see Eq. (78). The moments M_{xss1} and M_{yss1} are similarly defined from $\underline{M}_{ss1}$ which is associated with the terms in $\delta_g T_0$ of $\underline{M}_{ss}$. Finally, the quantities M_{xycc0} and M_{xycc1} are obtained in a similar fashion from $\underline{M}_{cc}$, Eq. (79).

2.2.3 Validation and Some Numerical Results

The mathematical developments presented in the two previous sections were validated by comparison with previously published results. In this respect, it should first be noted that the present higher order shear deformation plate theory formulation (HSDPT) naturally reduces to both the first order shear deformation plate theory (FSDPT) and the classical laminate plate theory (CPT) under the following assumptions:

$$\text{HSDPT} \rightarrow \text{FSDPT: } H(z) = z \quad \text{and} \quad R = A \quad X = W = C \quad \underline{\mu} = \underline{\theta} \tag{101}$$

$$\text{HSDPT} \rightarrow \text{CPT: } H(z) = 0 \quad \text{and} \quad R = X = W = 0 \quad \underline{\mu} = \underline{0}\ . \tag{102}$$

The present formulation was first validated by comparing the expressions for the parameters k_0, k_1, k_2, γ, and $\bar{p}_0$ obtained under the assumptions of Eq. (102) for a single layer isotropic plate with published CPT results (see Lee, 1993). After some algebraic manipulations, the exact values were recovered as

$$k_0 = \frac{\pi^4}{48} \frac{h^3 \left(a^2 + b^2\right)^2}{a^3 b^3} \frac{E}{1-\nu^2} \tag{103}$$

$$k_1 = -\alpha E \frac{\pi^2}{32} \frac{h\left(a^2 + b^2\right)}{ab} \tag{104}$$

$$k_2 = -\alpha \frac{\pi^2}{4} \frac{h\left(a^2 + b^2\right)}{ab} \frac{E}{1-\nu} \tag{105}$$

$$\gamma = \frac{\pi^4}{64} \frac{h}{a^3 b^3} \frac{E}{1-\nu^2} \left[\left(1-\nu^2\right)\left(a^4 + b^4\right) - 2\left(a^4 + b^4 + 2\nu a^2 b^2\right)\right] \tag{106}$$

$$p_0 = \alpha \frac{\pi^2}{48} \frac{h^2 \left(a^2 + b^2\right)}{ab} \frac{E}{1-\nu} \tag{107}$$

where α, E and ν are the coefficient of thermal expansion, Young's modulus and Poisson's ratio, respectively.

Next, the composite plate investigated by Kavallieratos (1992) was considered and the present CPT results were found to yield the values of the natural frequency ($\sqrt{k_0/M}\ /2\pi = 64.2695$ Hz) and buckling temperature ($-k_2/k_0 = 9.352$°F) stated by the author.

The validation of the FSDPT and HSDPT formulations was accomplished by comparing the results obtained by the present approach with those published by Reddy and Phan (1985) for three of their cases. Case I and II relate to single layers of a material

that is isotropic (for case I) and orthotropic (for case II) while in case III the plate is a 4 layer [0°/90°/90°/0°] composite. In all three cases, $a = b = 10h$. Shown in Table 1 is a comparison of the natural frequencies obtained by Reddy and Phan (1985) and by the present formulation. Note, in the work of Reddy and Phan, that the inertia associated with the in-plane displacements $u_0(x, y, t)$, $v_0(x, y, t)$ and shears $\varphi_u(x, y, t)$, $\varphi_v(x, y, t)$ is included. Thus, a perfect equality of results should not be expected but the close matching shown in Table 2.1 indicates that these inertia terms affect only slightly the transverse deflections as assumed here.

Table 2.1. Comparison of dimensionless frequencies obtained by Reddy and Phan (1985) and by the present formulation. Square plate with $a/h = 10$.

	CPT	FSDPT	HSDPT
Reddy & Phan (Case I, Table 1)	0.0955	0.0930	0.0931
Present	0.0955	0.0934	0.0930
Reddy & Phan (Case II, Table 2)	0.0493	0.0474	0.0474
Present	0.0492	0.0476	0.0473
Reddy & Phan (Case III, Table 3)	18.652	15.083	15.270
Present	18.738	15.535	15.054

Having validated the accuracy of the present formulation, it was desired to investigate the effects of plate thickness and shear deformations on the transverse deflections. It was first observed that only the coefficients k_0 and p_0 are affected by the choice of plate theory (CPT, FSDPT, or HSDPT) as the remaining ones depend solely on the in-plane stress field. Table 2.2 and 2.3 present the values of k_0 and p_0 for different variations of the plate considered by Kavallieratos (1992) composed of eight layers oriented at $[0°/45°/-45°/90°]_s$. The geometric and material properties were selected as a = 20 in., b = 8.2 in., $\rho = 1.302\,10^{-4}$ lb-sec^2/in^4, $E_{11} = 18.6\ 10^6$ psi, $E_{22} = 2.0\ 10^6$ psi,, $G_{12} = 0.8\ 10^6$ psi, and $\nu_{12} = 0.31$. The values of the shear moduli G_{13} and G_{23}, which are required by both the FSDPT and HSDPT, were not specified by Kavallieratos and thus they were selected equal to G_{12}. The plate thickness which was selected by this author as h = 0.0416 in. (or b/h = 197.12) was varied here to yield different ratios b/h, specifically b/h = 197.12, 50, 20, and 10. The different values of k_0 and p_0 are summarized in Table 2.2 and 2.3, respectively.

Table 2.2. Values of the stiffness k_0 according to different theories and for different thicknesses

b/h	CPT	FSDPT	HSDPT
197.12	36.212	36.206	36.204
50	2218.76	2212.77	2210.77
20	34668.10	34091.88	33903.71
10	277344.77	259844.26	254498.47

Table 2.3. Values of the force p_0 according to different theories and for different thicknesses

b/h	CPT	FSDPT	HSDPT
197.12	0.009336	0.009334	0.009334
50	0.1451	0.1447	0.1446
20	0.9069	0.8914	0.8869
10	3.6275	3.3921	3.3287

It is seen from the above tables that the three theories yield similar values of k_0 and $\bar{p}_0$ as long as *b/h* remains larger than 50 or so. As this ratio decreases, the difference between the classical plate theory and the shear deformation formulations steadily increases. At $b/h = 10$, the classical plate theory is approximately 10% away from HSDPT while the two shear deformation formulations differ from each other by only 2%.

2.3 Panel Displacement-Stress Relations

The structural dynamic modeling of composite panels accomplished above has focused on the determination of the differential equation for the dynamic response, i.e. the variable $q(t)$. In addition to this equation, the estimation of the fatigue life of these panels requires also the stress-displacement relations which are obtained as follows. First, the stresses at a certain depth z, $\underline{\sigma}(z)$, are related to the corresponding strains $\underline{\varepsilon}(z)$ through Eq. (8). Next, the strains $\underline{\varepsilon}(z)$ must be expressed in terms of the single modal displacement $q(t)$. This second step is accomplished by relying on the strains, curvatures and shear related terms $\underline{\varepsilon}^0$, $\underline{\kappa}$, $\underline{\phi}$, and $\underline{\phi}'$ defined in Eq. (28)-(30). Specifically, it can be shown that

$$\underline{\varepsilon}(z) = G(z) \begin{bmatrix} \underline{\varepsilon}^0 \\ \underline{\kappa} \\ \underline{\phi} \\ \underline{\phi}' \end{bmatrix} \tag{108}$$

where the 6x11 matrix $G(z)$ is

$$G(z) = \left[\begin{array}{ccc|ccc|cc|ccc} 1 & 0 & 0 & z & 0 & 0 & 0 & 0 & H(z) & 0 & 0 \\ 0 & 1 & 0 & 0 & z & 0 & 0 & 0 & 0 & H(z) & 0 \\ 0 & 0 & 0 & 0 & 0 & 0 & 0 & 0 & 0 & 0 & 0 \\ 0 & 0 & 0 & 0 & 0 & 0 & H'(z) & 0 & 0 & 0 & 0 \\ 0 & 0 & 0 & 0 & 0 & 0 & 0 & H'(z) & 0 & 0 & 0 \\ 0 & 0 & 1 & 0 & 0 & z & 0 & 0 & 0 & 0 & H(z) \end{array}\right] \tag{109}$$

It remains then to express the four vectors $\underline{\varepsilon}^0$, $\underline{\kappa}$, $\underline{\phi}$, and $\underline{\phi}'$ in terms of the modal displacement $q(t)$. To this end, note from previous developments, i.e. Eq. (33), that

$$\underline{\varepsilon}^0 = \widetilde{A}^{-1} \left[\underline{N} + \underline{N}^t\right] \tag{110}$$

in the case of a symmetric composite. This relation provides a direct connection between $\underline{\varepsilon}^0$ and $q(t)$ since the vector $\underline{N}^t$ and the matrix $\widetilde{A}$ are independent of this quantity, see Eq. (27) and (31), and the components N_x, N_y, and N_{xy} of $\underline{N}$ are specified by Eq. (52)-(54). Accordingly, the vector $\underline{\varepsilon}^0$ can be expressed as the sum of a constant term and a quadratic component in q, i.e.

$$\underline{\varepsilon}^0 = \underline{\varepsilon}_0^0 + \underline{\varepsilon}_2^0 \, q^2 \, . \tag{111}$$

Turning next to the curvatures, $\underline{\kappa}$, the assumed transverse displacement

$$w_0(x,y) = q \sin\frac{\pi x}{a} \sin\frac{\pi y}{b} \tag{112}$$

implies that

$$\underline{\kappa} = q \begin{bmatrix} \dfrac{\pi^2}{a^2} \sin\dfrac{\pi x}{a} \sin\dfrac{\pi y}{b} \\ \dfrac{\pi^2}{b^2} \sin\dfrac{\pi x}{a} \sin\dfrac{\pi y}{b} \\ -\dfrac{2\pi^2}{a\,b} \cos\dfrac{\pi x}{a} \cos\dfrac{\pi y}{b} \end{bmatrix} . \tag{113}$$

Finally, the shear related terms $\underline{\phi}$ and $\underline{\phi}'$ are readily evaluated from Eq. (64), (65), and (67) where the vector $\underline{R}_p$ is obtained by solving the system of equations (75). These relations demonstrate that both $\underline{\phi}$ and $\underline{\phi}'$ depend linearly on q, i.e.

$$\underline{\phi} = \underline{\phi}_0 + \underline{\phi}_1 \, q \qquad \text{and} \qquad \underline{\phi}' = \underline{\phi}_0{}' + \underline{\phi}_1{}' \, q . \qquad (114), (115)$$

Then, combining Eq. (8), (108), (111), and (113)-(115), it is found that the stress vector at any point can be expressed as

$$\underline{\sigma} = \underline{\sigma}_0 + \underline{\sigma}_1 \, q + \underline{\sigma}_2 \, q^2 . \qquad (116)$$

2.4 Non-Dimensionalization of the Structural Dynamics Equations

In order to compare the effects of the acoustic excitation on different composite and isotropic panels, it is convenient to first rewrite the governing equation for the transverse displacement q and the stress-displacement relations in dimensionless forms. For the former, consider the differential equation, Eq. (95), and introduce the dimensionless displacement $\hat{q}$ and time τ defined as

$$\hat{q} = \frac{q}{2h} \qquad (117)$$

and

$$t = \theta \tau \qquad (118)$$

where θ is an appropriate time constant. Introducing these new variables in Eq. (95) leads to

$$\ddot{\hat{q}} + \frac{\theta^2}{M} k_0 (1 - s) \hat{q} + \frac{4 \theta^2 \gamma h^2}{M} \hat{q}^3 = \frac{\theta^2 p_0}{2M h} + \frac{\theta^2}{2M h} p(\theta\tau) \qquad (119)$$

where

$$s = -\frac{k_1 \delta_v + k_2}{k_0} T_0 \qquad (120)$$

is the ratio of the panel temperature to the buckling temperature. Equation (119) is of the same form (without the damping term) as the one considered by Lee (1993) in connection with isotropic panels provided that

$$\frac{\theta^2}{M} k_0 = \omega_0^2 = \left(1 + \frac{b^2}{a^2}\right)^2 . \qquad (121)$$

Accordingly, the time parameter θ will be selected as

$$\theta = \left(1 + \frac{b^2}{a^2}\right) \sqrt{\frac{M}{k_0}} . \qquad (122)$$

Then, the nonlinear term is $\hat{\gamma} \, \hat{q}^3$ with

$$\hat{\gamma} = \frac{4 \theta^2 \gamma h^2}{M} \qquad (123)$$

and the constant effect of the temperature gradients is

$$\bar{p}_0 = \frac{\theta^2 p_0}{2M h} . \qquad (124)$$

Finally, the normalized acoustic excitation $\bar{p}(\tau)$ can be written as

$$\bar{p}(\tau) = \frac{\theta^2}{2M\,h}\,p(\theta\tau) \tag{125}$$

so that its power spectral density is

$$S_{\bar{p}\bar{p}}(\omega) = \frac{\theta^4}{4\,M^2\,h^2}\,\frac{S_{pp}\left(\frac{\omega}{\theta}\right)}{\theta} = \frac{\theta^3}{4\,M^2\,h^2}\,S_{pp}\left(\frac{\omega}{\theta}\right). \tag{126}$$

Note in the isotropic case that the above expressions reduce to the relations obtained by Lee (1993) and used in the previous reports. Accordingly, it is desired that the normalization of the stress coefficients also yields their isotropic forms which were obtained by factoring the common term $E\,\frac{\pi^2\,h^2}{b^2}$. Paralleling this effort, let

$$\underline{\sigma} = E_{eq}\,\frac{\pi^2\,h^2}{b^2}\left(\underline{C}_0 + \underline{C}_1\,\hat{q} + \underline{C}_2\,\hat{q}^2\right) \tag{127}$$

where the coefficient vectors $\underline{C}_0$, $\underline{C}_1$, and $\underline{C}_2$ are defined as

$$\underline{C}_0 = \frac{b^2}{\pi^2\,E_{eq}\,h^2}\,\underline{\sigma}_0 \tag{128}$$

$$\underline{C}_1 = \frac{2\,b^2}{\pi^2\,E_{eq}\,h}\,\underline{\sigma}_1 \tag{129}$$

and

$$\underline{C}_2 = \frac{4\,b^2}{\pi^2\,E_{eq}}\,\underline{\sigma}_2 \quad . \tag{130}$$

To complete this normalization, it remains to specify an "equivalent" Young's modulus E_{eq}. Relying on the definition of k_0 for isotropic panels, it is suggested here that

$$E_{eq} = \frac{48}{\pi^4}\,\frac{a^3 b^3}{h^3\left(a^2+b^2\right)^2}\left(1-\nu_{12}\,\nu_{21}\right)k_0. \tag{131}$$

2.5 The Prototypical Equation

The derivations of the previous sections have demonstrated that the structural dynamic response of the panels, composite or isotropic, is governed by the same equations, i.e.

$$\ddot{q} + 2\,\zeta\,\dot{q} + \omega_0^2\,(1-s)\,q + \gamma\,q^3 = \bar{p}_0 + \bar{p}(t) \tag{132}$$

for the displacements and Eq. (127) for the stresses. Accordingly, most of the ensuing discussion will focus on a single example of application without lack of generality. Specifically, the clamped isotropic titanium plate already investigated by Vacaitis (1994) will be reconsidered here. The dimensions of the panel were selected as a = 8.2 in, b = 20.0 in, and h = 0.06 in. The acoustic excitation was assumed to be a white noise random process (uncorrelated fluctuations over time but fully correlated over space) of

spectral density $S_0 = \frac{p_0^2}{2\pi} 10^{SPL/10}$ where $p_0 = 2.910^{-9}$ psi is the reference pressure and SPL denotes the sound pressure level in dB. The panel was assumed to be subjected to a uniform temperature increase of T_0 so that the constant term $\bar{p}_0$ in Eq. (132) vanishes. Then, in their dimensionless forms (see Lee, 1993), the parameters of Eq. (132) and (127) can be expressed as

$$\omega_0^2 = \frac{16}{3}\left(\beta^4 + 2\beta^2/3 + 1\right) \tag{133}$$

$$s = T_0 \tag{134}$$

$$\gamma = \frac{32\beta^2}{3}\left\{\beta^2 + \beta^{-2} + 2\nu + \frac{4}{9}\left(1-\nu^2\right)\left[\frac{17}{8}\left(\beta^2 + \beta^{-2}\right) + 4\left(\beta + \beta^{-1}\right)^{-2} + \left(4\beta + \beta^{-1}\right)^{-2} + \left(\beta + 4\beta^{-1}\right)^{-2}\right]\right\} \tag{135}$$

$$C_0(x, y, z) = -\frac{\left(\beta^4 + 2\beta^2/3 + 1\right)}{3\left(1-\nu^2\right)\left(\beta^2 + 1\right)} T_0 \tag{136}$$

$$C_1(x, y, z) = -\frac{16\bar{z}\left(\beta^2 \cos 2\pi\bar{x} \sin^2 \pi\bar{y} - \nu \sin^2 \pi\bar{x} \cos 2\pi\bar{y}\right)}{3\left(1-\nu^2\right)} \tag{137}$$

$$C_2(x, y, z) = \frac{2\left(\beta^2 + \nu\right)}{3\left(1-\nu^2\right)} - \frac{32}{9}\left\{\frac{\beta^2 \cos 2\pi\bar{y}}{4} - \frac{\beta^2 \cos 4\pi\bar{y}}{16}\right\}$$

$$-\frac{32}{9}\left\{-\frac{\cos 2\pi\bar{x} \cos 2\pi\bar{y}}{2\left(\beta + \beta^{-1}\right)^2} + \frac{\cos 2\pi\bar{x} \cos 4\pi\bar{y}}{\left(\beta + 4\beta^{-1}\right)^2} + \frac{\cos 4\pi\bar{x} \cos 2\pi\bar{y}}{4\left(4\beta + \beta^{-1}\right)^2}\right\} \tag{138}$$

where $\beta = b/a$, $\bar{x} = x/a$, $\bar{y} = y/b$, $\bar{z} = z/h$. Further, the damping ratio ζ and Poisson's ratio ν were set to 0.01 and 0.34, respectively. Finally, in the above dimensionless form the power spectral density of the white noise pressure term $\bar{p}(t)$ is expressed as

$$S_{\bar{p}\bar{p}} = 144\left(\frac{b}{\pi h}\right)^8 \frac{\left(1-\nu^2\right)^2}{E^2} \frac{4}{9} \frac{S_0}{\theta} \tag{139}$$

where

$$\theta = \sqrt{\frac{12\left(1-\nu^2\right)}{\pi^4} \frac{\rho b^4}{E h^2}}\,. \tag{140}$$

The numerical integration of the equation of motion, Eq. (132) proceeded as follows. First, an estimate of the time scale in the fluctuations of the process $q(t)$ was obtained by considering the undamped linear natural frequency ω_0 and a time step of $0.2/\omega_0$ was set for the numerical integration of Eq. (132). This selection implied a

maximum (Nyquist) frequency (see Oppenheim and Schafer, 1975, for a discussion) of $\omega_b = 5\,\pi\,\omega_0$ so that both the acoustic excitation $\bar{p}(t)$ and its corresponding panel response $q(t)$ were defined in the frequency interval $\omega \in [-\omega_b, \omega_b]$. Then, the constant value of the acoustic loading in the n^{th} time step, $\bar{p}_n$, was generated according to its specified power spectrum (see Mignolet, 1993, for some fast algorithms to accomplish this computation). If the excitation process is white noise with constant power spectral density S_0, then the samples $\bar{p}_n$ form a sequence of independent random numbers with common mean, $E\left[\bar{p}_n\right] = 0$, and variance $E\left[\bar{p}_n^2\right] = 10\,\pi\,\omega_0\,S_0$. Next, Eq. (132) was numerically integrated with the specified time step by a Runge-Kutta-Verner of orders five and six (IMSL routine DIVPRK). Finally, the discrete values of the response deflection $q(t)$ were used to produce the time histories of the stresses according to Eq. (127).

The results of this numerical integration are shown in Fig. 2.2-2.13. A few preliminary observations can be drawn from these figures. First, note the clear nonlinearity of the displacement-stress relation in the neighborhood of the bottom buckling state. Indeed, although the displacement time histories corresponding to sound pressure levels of 119 and 134 dB are fairly symmetric with respect to this level, the stresses are not, exhibiting a definite "bottoming out". That is, during the excursions of the panel around this position, the stress process achieves a minimum value dictated by the quadratic relation (127). This peculiarity is not encountered around the top buckling position since Eq. (127) remains monotonic in this region.

A different perspective on the behavior of the displacements can be gathered from the power spectral density plots of Fig. 2.8-2.10. In particular, it is observed that this spectrum exhibits only one peak at a sound pressure level of 104dB, corresponding to the fluctuations around the buckling states. As the *SPL* increases, so does the amplitude of the motions and the response exhibits increasingly nonlinear features, as the second dominant frequency shown in Fig. 2.9 for a *SPL* of 119dB. Note that this second frequency appears to be a subharmonic of order 1/2 of the "fundamental". Finally, at still higher *SPL*, see Fig. 2.10 for *SPL* = 134dB, the displacement process has lost its narrowbandedness and exhibits a single, rather wide peak.

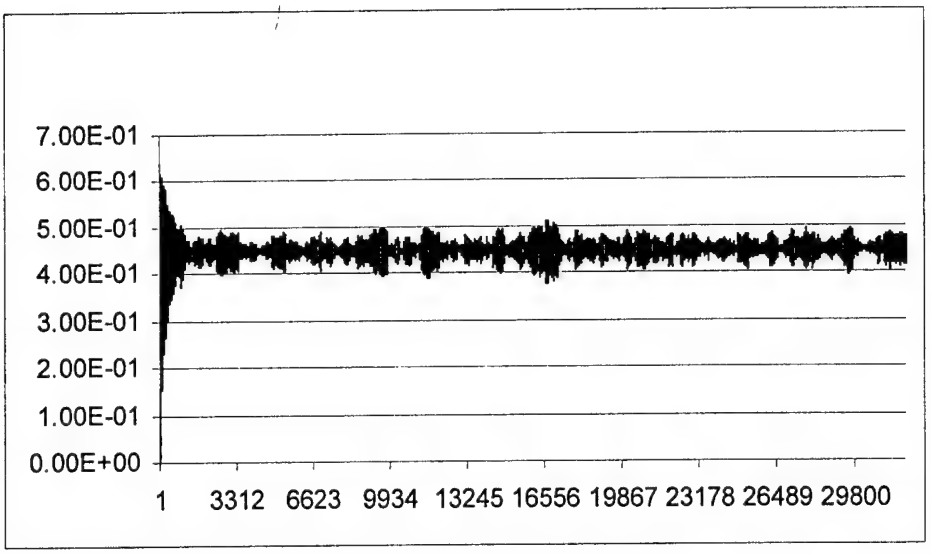

Figure 2.2 Time history of the displacement, $s = 1.8$, $SPL = 104$dB

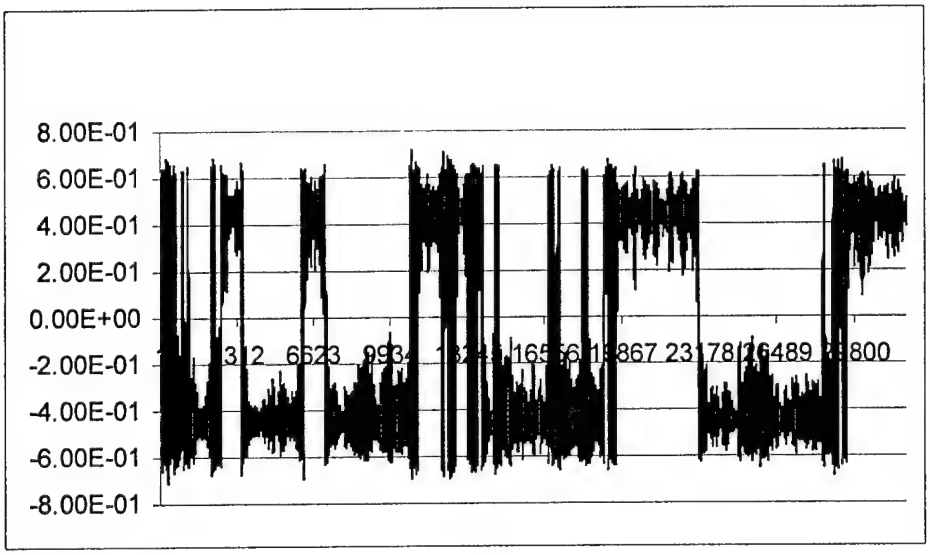

Figure 2.3 Time history of the displacement, $s = 1.8$, $SPL = 119$dB

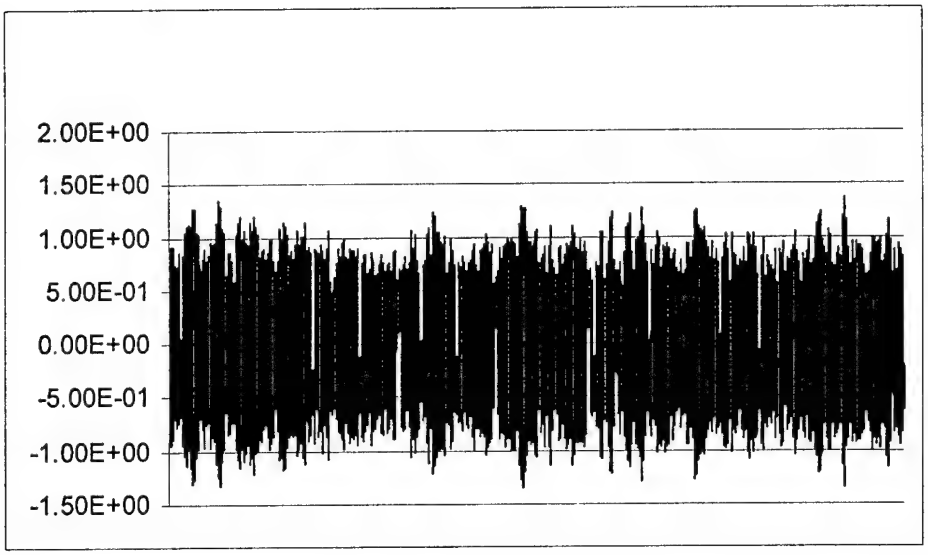

Figure 2.4 Time history of the displacement, $s = 1.8$, $SPL = 134$dB

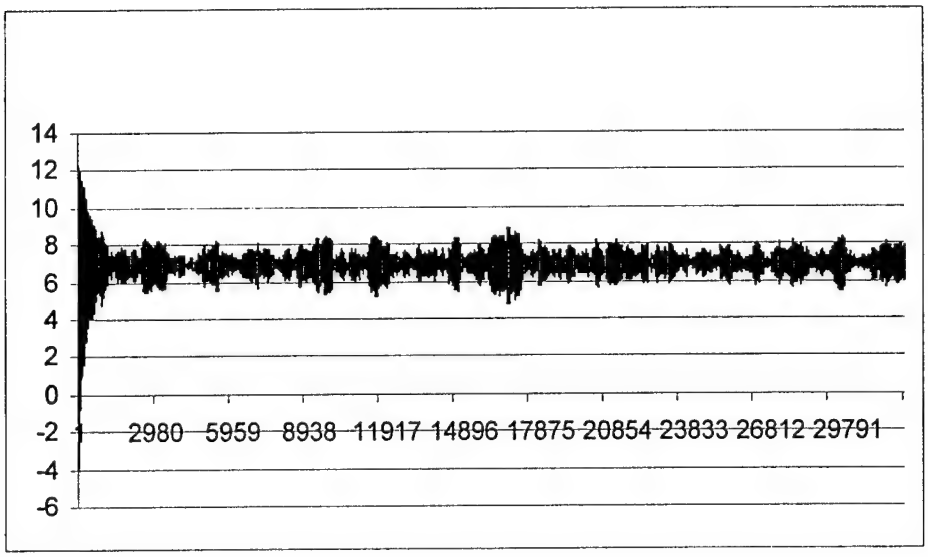

Figure 2.5 Time history of the stress, $s = 1.8$, $SPL = 104$dB

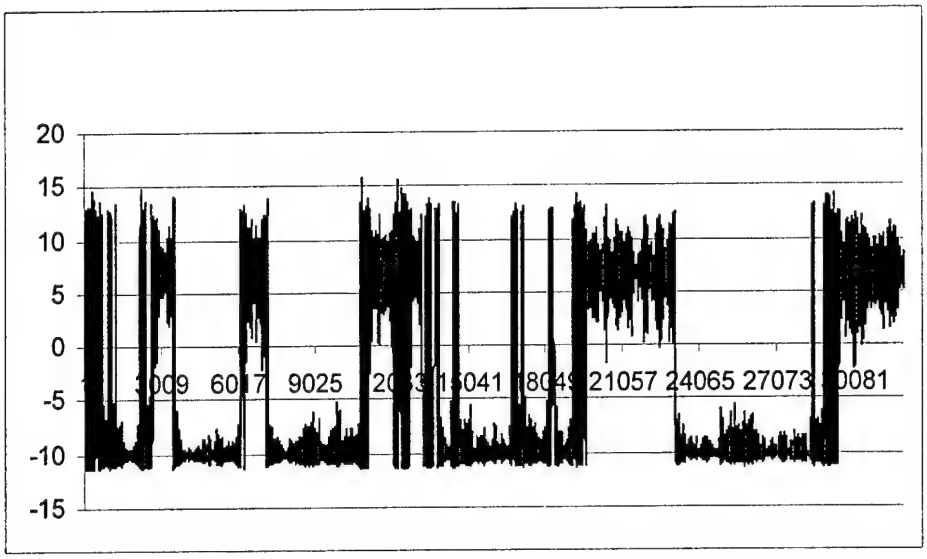

Figure 2.6 Time history of the stress, $s = 1.8$, $SPL = 119$dB

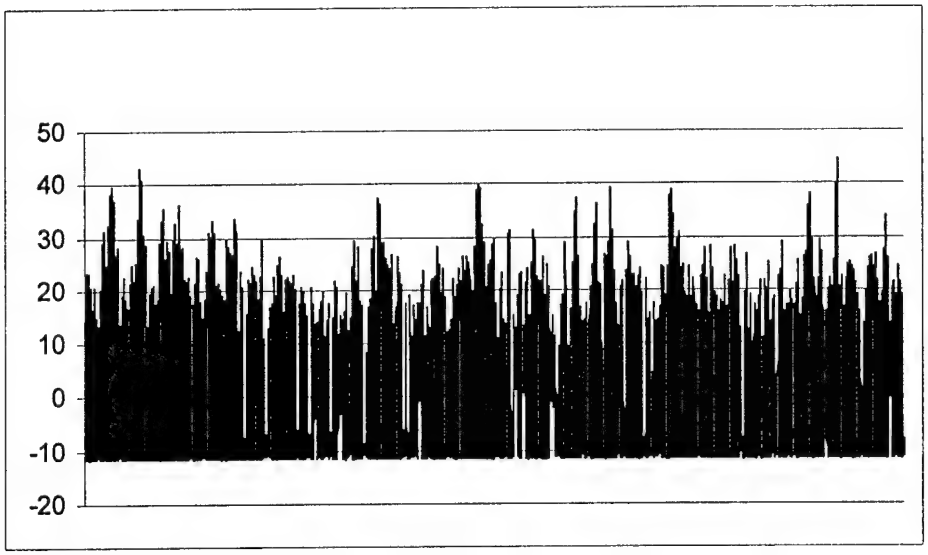

Figure 2.7 Time history of the stress, $s = 1.8$, $SPL = 134$dB

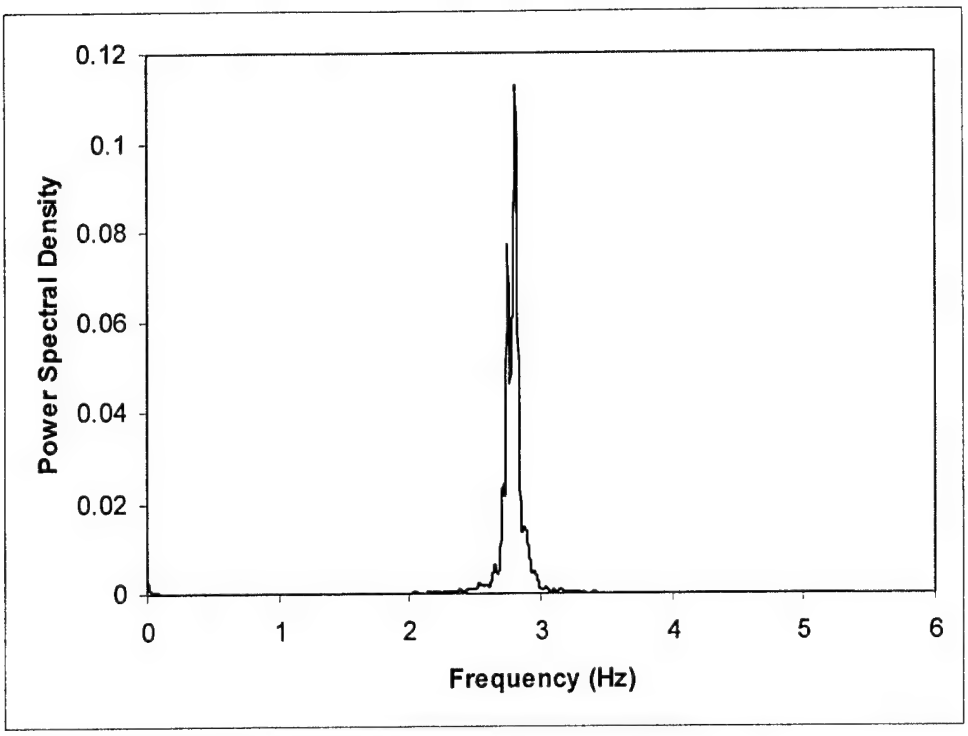

Figure 2.8 Power spectral density of the displacement process, $s = 1.8$, $SPL = 104$dB

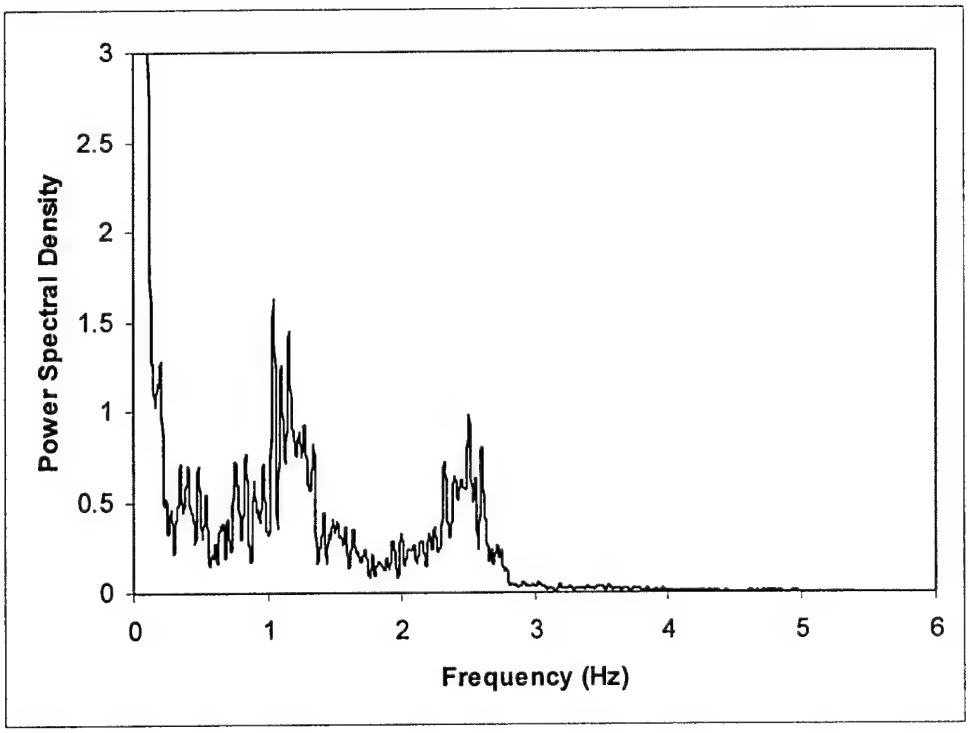

Figure 2.9 Power spectral density of the displacement process, $s = 1.8$, $SPL = 119$dB

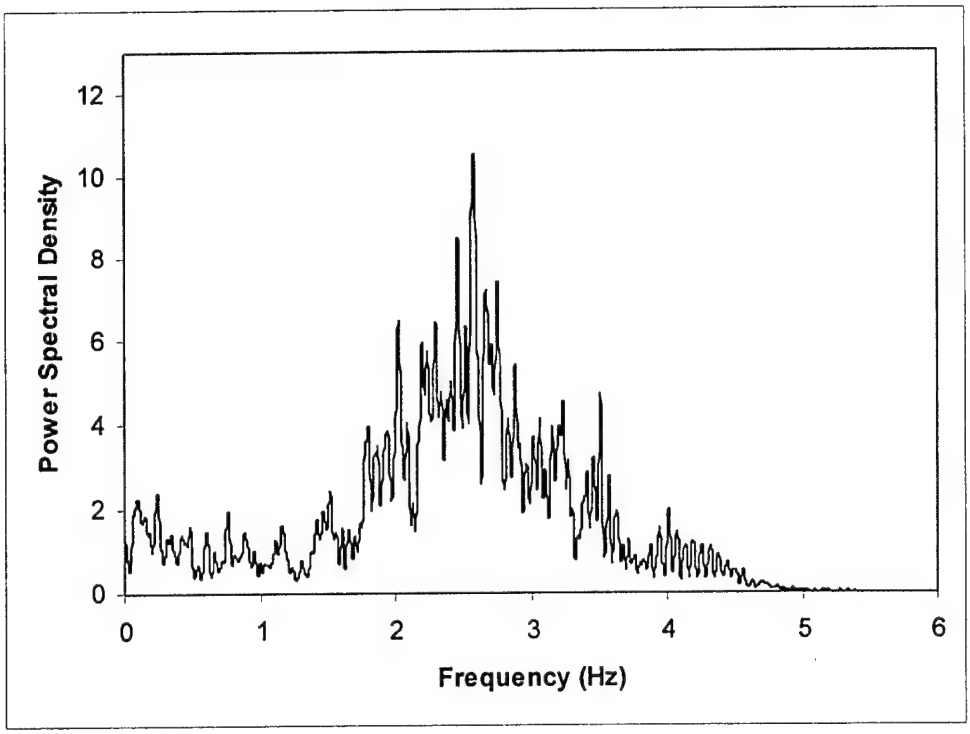

Figure 2.10 Power spectral density of the displacement process, $s = 1.8$, $SPL = 134$dB

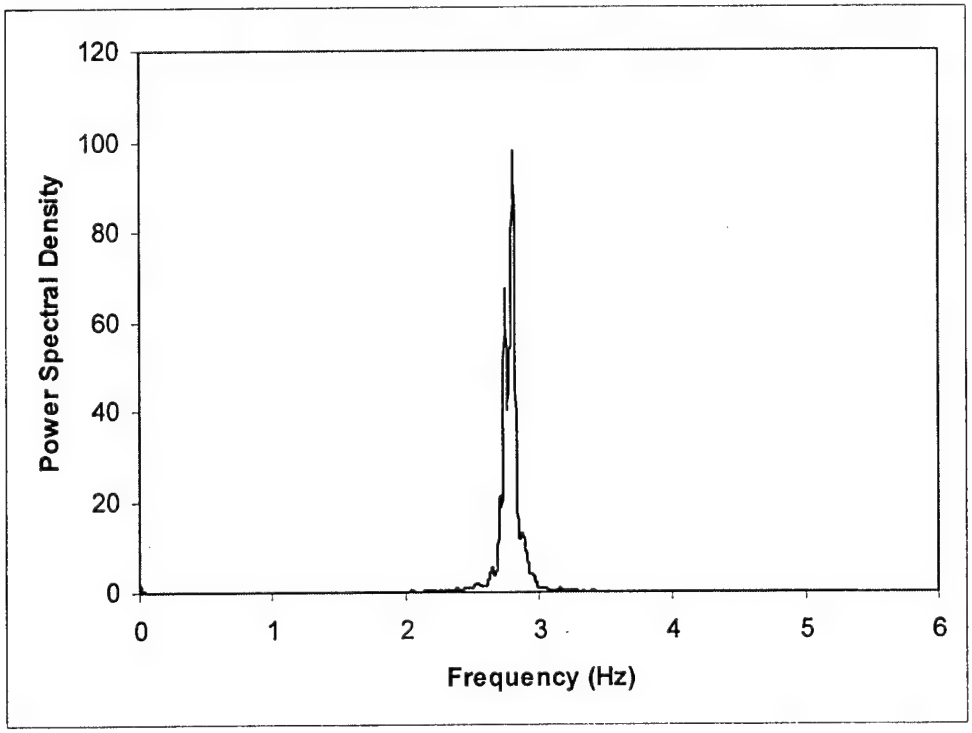

Figure 2.11 Power spectral density of the stress process, $s = 1.8$, $SPL = 104$dB

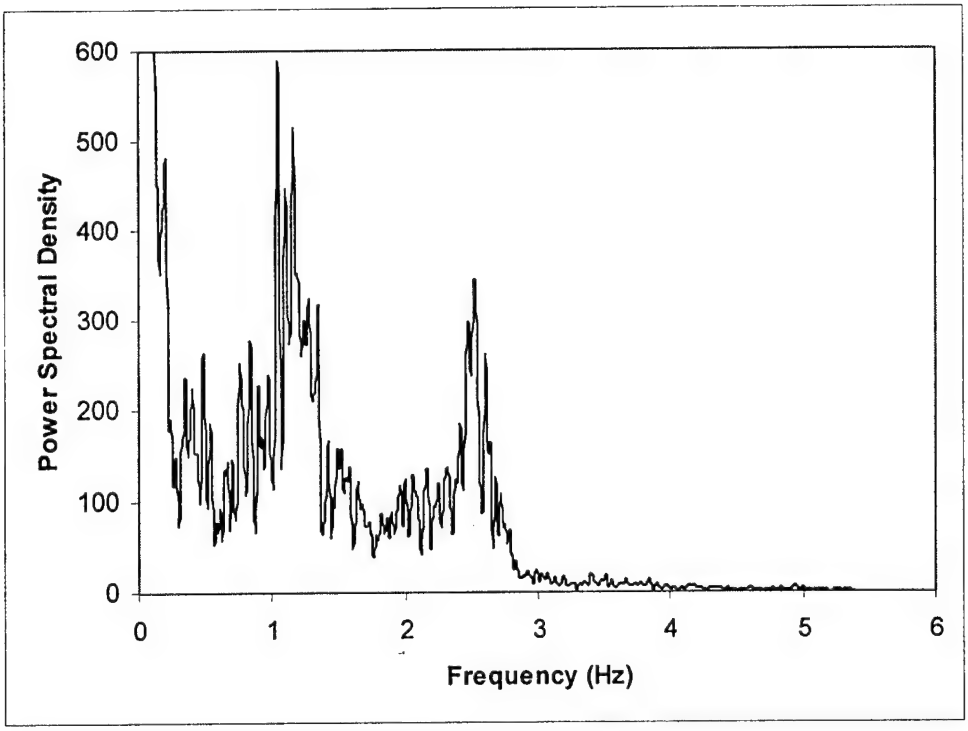

Figure 2.12 Power spectral density of the stress process, $s = 1.8$, $SPL = 119$dB

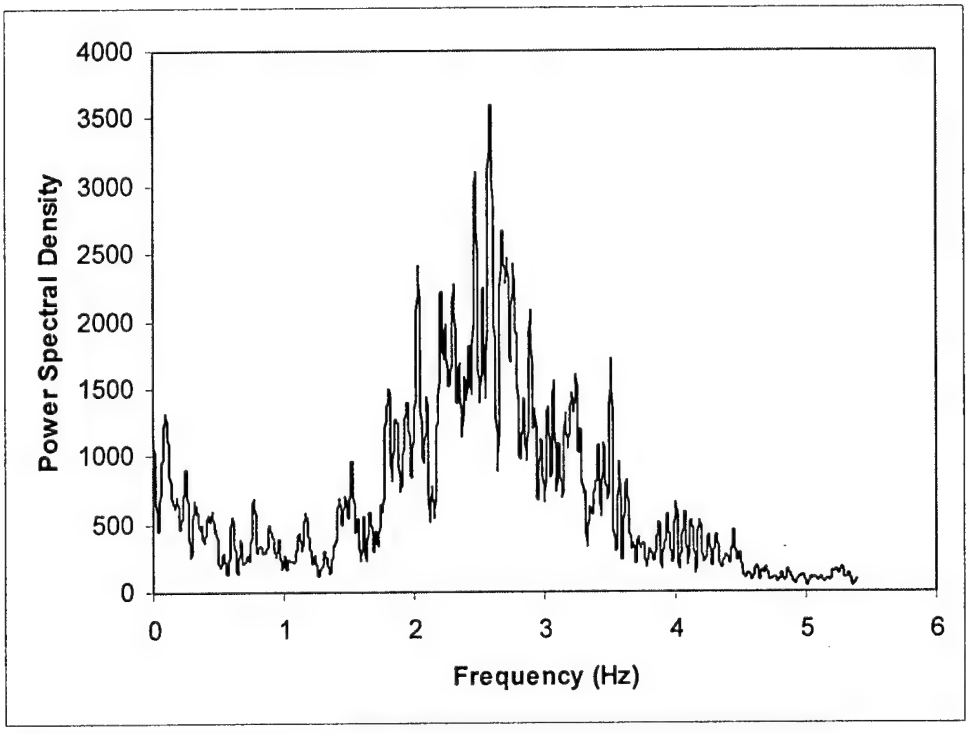

Figure 2.13 Power spectral density of the stress process, $s = 1.8$, $SPL = 134$dB

SECTION 3
EQUIVALENT LINEARIZATION TECHNIQUES

The estimation of the fatigue life of the panels can be viewed as a two-step process. Indeed, it is first necessary to evaluate the statistical characteristics of the dynamic response, i.e. of the displacement $q(t)$ and velocity $\dot{q}(t)$ satisfying the nonlinear stochastic differential equation (132). In the second stage, the damage generated by the stresses, see Eq. (127), is then estimated from the known moments of $q(t)$ and $\dot{q}(t)$.

The determination of the *exact* values of the moments of the displacement $q(t)$ and the velocity $\dot{q}(t)$ satisfying Eq. (132) and corresponding to a white noise excitation $\bar{p}(t)$ is easily accomplished by relying on the joint probability density function of these two random variables, as given by Lutes and Sarkani (1997). The availability of this distribution is however rather accidental as Eq. (132) belongs to a limited class of stochastic differential equations for which an exact solution of the Fokker-Planck equation can be obtained. For example, such a closed form solution is unavailable if the acoustic excitation $\bar{p}(t)$ is a colored noise. Further, known expressions for the joint distribution of the solution of a system of stochastic differential equations, as would be obtained for example in a multiple mode analysis of the panel, are extraordinarily limited. These comments clearly indicate that the development of a general strategy for the estimation of the fatigue life of the panels cannot rely on exact expressions for the joint probability density function of the displacements and velocities. Rather, it is necessary to rely on an alternate, general purpose methodology for the estimation of the moments of $q(t)$ and $\dot{q}(t)$. To this end, the equivalent linearization method (see Roberts and Spanos, 1990) will be used.

According to this methodology, the nonlinear equation (132) is replaced by an "equivalent linear" one of the form

$$\ddot{q} + 2\zeta\omega_0\,\dot{q} + k_{eq}\,q = \bar{p}_{eq} + \bar{p}(t) \tag{141}$$

where the parameters k_{eq} and $\bar{p}_{eq}$ are selected so that Eq. (141) represents "at best" Eq. (132). Specifically, these coefficients will be chosen so that the modeling error

$$E_{\text{mod}} = E\left[\left\{\left(\omega_0^2\,(1-s)\,q + \gamma\,q^3 - \bar{p}_0\right) - \left(k_{eq}\,q - \bar{p}_{eq}\right)\right\}^2\right] \tag{142}$$

where $E[\ ]$ denotes the operator of mathematical expectation, is minimized.

3.1 Equivalent Linearization Strategy #1

Proceeding with a differentiation of E_{mod} with respect to $\bar{p}_{eq}$ and k_{eq} yields, respectively,

$$\omega_0^2\,(1-s)\,\mu_q + \gamma\,E\left[q^3\right] - \bar{p}_0 - k_{eq}\,\mu_q + \bar{p}_{eq} = 0 \tag{143}$$

$$\omega_0^2\,(1-s)\left(\sigma_q^2 + \mu_q^2\right) + \gamma\,E\left[q^4\right] - \bar{p}_0\,\mu_q - k_{eq}\left(\sigma_q^2 + \mu_q^2\right) + \bar{p}_{eq}\,\mu_q = 0 \tag{144}$$

where μ_q and σ_q^2 denote the mean and variance of $q(t)$, i.e. $\mu_q = E[q]$ and $\sigma_q^2 = E\left[(q-\mu_q)^2\right]$. It is clearly seen from Eq. (143) and (144) that the evaluation of the parameters k_{eq} and $\bar{p}_{eq}$ requires the knowledge of the yet unknown moments μ_q and σ_q^2. This indetermination is resolved by replacing the exact values of the mean μ_q and variance σ_q^2 of the displacement $q(t)$ satisfying Eq. (132) by those associated with the solution of the linear differential equation (141). Specifically, following standard random vibration arguments (see Lutes and Sarkani, 1997), it is found that

$$\mu_q = \frac{\bar{p}_{eq}}{k_{eq}} \qquad \text{and} \qquad \sigma_q^2 = \frac{\pi S_{\bar{p}\bar{p}}}{2\zeta\omega_0 k_{eq}} \qquad (145), (146)$$

Then, the solution of the four coupled nonlinear algebraic equations (143)-(146) yields the values of μ_q, σ_q^2, $\bar{p}_{eq}$, and k_{eq}. Of primary interest here are the two moments and thus, eliminating $\bar{p}_{eq}$, and k_{eq} from the above equations yields

$$\omega_0^2 (1-s)\mu_q + \gamma E\left[q^3\right] = \bar{p}_0 \qquad (147)$$

$$\omega_0^2 (1-s)\left(\sigma_q^2 + \mu_q^2\right) + \gamma E\left[q^4\right] = \bar{p}_0 \mu_q + \frac{\pi S_{\bar{p}\bar{p}}}{2\zeta\omega_0}. \qquad (148)$$

Note further that the evaluation of the mean and variance is accomplished on the basis of the linear stochastic differential equation (141) or equivalently under the assumption that $q(t)$ is a Gaussian random process. Then, proceeding consistently, the third and fourth order moments appearing in Eq. (147) and (148) can be expressed as

$$E\left[q^3\right] = 3\mu_q \sigma_q^2 + \mu_q^3 \qquad (149)$$

and

$$E\left[q^4\right] = 3\sigma_q^4 + 6\mu_q^2 \sigma_q^2 + \mu_q^4. \qquad (150)$$

In solving Eq. (147)-(150) for the required moments μ_q and σ_q^2, two separate cases must be considered, i.e. $\mu_q \neq 0$ and $\mu_q = 0$. Since the latter condition is possible only when $\bar{p}_0 = 0$, the analysis will focus separately on the panels experiencing a temperature gradient through the thickness ($\bar{p}_0 \neq 0$) or a lack thereof ($\bar{p}_0 = 0$).

3.1.1 Equivalent Linearization Results: $\bar{p}_0 \neq 0$

After some algebraic manipulations (including a multiplication of Eq. (147) and (148) by μ_q^2), it is found that the mean value μ_q satisfies the following sixth order algebraic equation

$$2\gamma^2\mu_q^6+2\gamma\omega_0^2(1-s)\mu_q^4-\bar{p}_0\gamma\mu_q^3+3\gamma\left(\frac{\pi S_{pp}^{--}}{2\zeta\omega_0}\right)\mu_q^2+\bar{p}_0\omega_0^2(1-s)\mu_q-\bar{p}_0^2=0. \tag{151}$$

Once the value of μ_q has been obtained from the above equation, the variance σ_q^2 can be evaluated from Eq. (147) and (149) as

$$\sigma_q^2=\frac{\left[\bar{p}_0-\omega_0^2(1-s)\mu_q-\gamma\mu_q^3\right]}{3\gamma\mu_q} \tag{152}$$

3.1.2 Equivalent Linearization Results: $\bar{p}_0=0$

When $\bar{p}_0=0$, Eq. (147) admits a symmetric solution of the form $\mu_q=0$ but this solution is not necessarily the only one so that the two separate sub-cases $\bar{p}_0=0;\mu_q\neq 0$ and $\bar{p}_0=0;\mu_q=0$ must be investigated.

1.1.B.1 Sub-case #1: $\bar{p}_0=0;\mu_q\neq 0$

If the solution $\mu_q=0$ is not desired, the algebraic manipulations carried out in connection with the derivation of Eq. (151) can be repeated to yield

$$2\gamma\mu_q^4+2\omega_0^2(1-s)\mu_q^2+3\left(\frac{\pi S_{pp}^{--}}{2\zeta\omega_0}\right)=0 \tag{153}$$

so that

$$\mu_q^2=\frac{1}{2\gamma}\left[-\omega_0^2(1-s)\pm\sqrt{\omega_0^4(1-s)^2-6\gamma\frac{\pi S_{pp}^{--}}{2\zeta\omega_0}}\right]. \tag{154}$$

Once the value of μ_q has been obtained from the above equation, the variance σ_q^2 can be evaluated from Eq. (152) as

$$\sigma_q^2=\frac{-\omega_0^2(1-s)-\gamma\mu_q^2}{3\gamma}. \tag{155}$$

The above solutions, Eq. (154) and (155), exhibit some very interesting features. In particular, in the limit of a zero acoustic excitation $S_{pp}^{--}\to 0$, the mean value converges toward the buckling states Q_1 and Q_2. Further, if $s<1$, i.e. when the thermal effects are not sufficient to buckle the plate, there is no positive value of μ_q^2 in Eq. (154) so that no solution of this type exists. Finally, the existence of μ_q requires the term inside the square root to be positive, or equivalently that $\omega_0^4(1-s)^2-6\gamma\frac{\pi S_{pp}^{--}}{2\zeta\omega_0}\geq 0$. This

inequality implies that a nonzero mean is not possible when the acoustic level exceeds a certain threshold. Numerical results indicate that this threshold closely match the sound pressure level (*SPL*) at which the snap-throughs become very frequent.

1.1.B.2 Sub-case #2: $\bar{p}_0 = 0 ; \mu_q = 0$

On the contrary of the mean value given by Eq. (154), the solution $\mu_q = 0$ always exists when $\bar{p}_0 = 0$ since Eq. (147) and (149) are identically satisfied. The corresponding value of the variance is then given by Eq. (148) and (150), that is

$$\sigma_q^2 = \frac{1}{6\gamma}\left[\sqrt{\omega_0^4 (1-s)^2 + 6\gamma \frac{\pi S_{pp}^{--}}{\zeta \omega_0}} - \omega_0^2 (1-s)\right]. \tag{156}$$

3.2 Equivalent Linearization Strategy #2

It is known (see Lutes and Sarkani, 1997, for example) that the exact probability density function of the displacement $q(t)$ is bimodal for all values of the sound pressure level, or equivalently for all values of S_{pp}^{--}, provided that $s \geq 1$. The equivalent linearization formulation developed above is consistent with this property as long as there exist mean values satisfying Eq. (151) or (154). For larger values of the sound pressure level, however, the above equivalent linearization fails to accurately capture this property, for example, for $\bar{p}_0 = 0$ and S_{pp}^{--} large enough the only acceptable mean value μ_q is zero and the bimodal character is lost. To recover this important property, it is suggested here to proceed with a different equivalent linearization formulation in which the mean is imposed to be different from zero and the standard deviation is obtained to minimize the modeling error of Eq. (142). Physical arguments motivate the selection of the imposed mean values to be the buckled states, i.e. $\mu_q = Q_1$ or $\mu_q = Q_2$, where

$$\omega_0^2 (1-s) Q_i + \gamma Q_i^3 = 0 \qquad Q_i \neq 0 \qquad i = 1, 2. \tag{157}$$

Accordingly, Eq. (145) requires that

$$\bar{p}_{eq} = k_{eq} Q_i \tag{158}$$

so that the modeling error, Eq. (142), can be rewritten as

$$E_{\text{mod}} = E\left[\left\{\left(\omega_0^2 (1-s) q + \gamma q^3 - \bar{p}_0\right) - k_{eq} (q - Q_i)\right\}^2\right]. \tag{159}$$

Differentiating the above expression with respect to the remaining parameter, k_{eq}, yields the equation

$$\omega_0^2 (1-s) E[q (q - Q_i)] + \gamma E\left[q^3 (q - Q_i)\right] - k_{eq} E\left[(q - Q_i)^2\right] = 0. \tag{160}$$

Then, using Eq. (146), (149), and (150), it can be shown that the above relation reduces to the following equation for the variance of q,

$$3\gamma \sigma_q^4 + \left[3\gamma Q_i^2 + \omega_0^2 (1-s)\right]\sigma_q^2 - \frac{\pi S_{pp}^{--}}{2\xi \omega_0} = 0 \tag{161}$$

the solution of which is

$$\sigma_q^2 = \frac{-\left[3\gamma Q_i^2 + \omega_0^2 (1-s)\right] + \sqrt{\left[3\gamma Q_i^2 + \omega_0^2 (1-s)\right]^2 + 6\gamma \dfrac{\pi S_{pp}}{\xi \omega_0}}}{6\gamma}. \qquad (162)$$

Note that this solution always exists for $s \geq 1$ as expected from the bimodal character of the exact probability density function.

3.3 Numerical Results

The prototypical problem analyzed in the previous section was reconsidered here to assess the validity and accuracy of the equivalent linearization strategies. For simplicity, it was again assumed that the effects of the gradient through the thickness are negligible so that $\bar{p}_0 = 0$.

Then, shown in Fig. 3.1 are the standard deviations of the displacement q obtained by Monte Carlo simulation of the fully nonlinear equation Eq. (132) and by the equivalent linearization strategies #1 and #2 for $s = 1.8$ as a function of the sound pressure level (*SPL*) in dB. The behavior of the Monte Carlo results is particularly informative, at very low *SPL* the panel vibrates with a very low amplitude around one of the buckled states. Since these two positions are equally probable and equally distant from the undeformed position q = 0, the overall mean is zero and the corresponding standard deviation should be very close to Q_1, as confirmed by Fig. 3.1 (for $s = 1.8$, Q_1 = 0.448). As the sound pressure level increases however, two different phenomena occur. First, the level of vibration around the buckled states increases slightly and unsymmetrically, i.e. the vibrations are larger toward the undeformed position because of the decreased local stiffness exhibited by the restoring forces. This lack of symmetry of the response induces a decrease of the mean displacement of the motions around each of the buckled states, i.e. $\mu_1 < Q_1$. The second effect is the appearance of snap-throughs, although very infrequent at first, that populate the region in between the two buckled states. Both of these factors imply the decrease of the standard deviation seen in Fig. 3.1. This process continues until the response becomes dominated by the snap-throughs in which case an increase in the excitation level mainly induces an increase in the level of response, i.e. the maximum displacement away from the undeformed position. Correspondingly, the standard deviation then starts increasing as a function of the sound pressure level as shown in Fig. 3.1. These observations would tend to confirm the earlier conjecture that the motion at low *SPL* is governed by the fluctuation processes only while at high excitation levels it is the snap-throughs that dictate the panel response. More importantly, it would appear that the region in which both of these processes are important is quite narrow and is located near the minimum of the standard deviation.

Table 3.1. Maximum value of the sound pressure level for which nonzero mean equivalent linearization solutions exist as a function of temperature s.

s	1.05	1.8	3	5
SPL (dB)	97	120	129	135

Considering next the equivalent linearization results, note first that when nonzero mean solutions exists, the corresponding overall standard deviation can be computed as

$$\sigma_q = \sqrt{\frac{1}{2}\left(\mu_1^2 + \sigma_1^2 + \mu_2^2 + \sigma_2^2\right)}. \tag{163}$$

Next, on the basis of physical arguments, the equivalent linearization results corresponding to the first approach were obtained for "low" SPL, i.e. for sound pressure levels lower than the threshold values given in Table 3.1, by the combination of the models associated with nonzero mean values μ_q closest to Q_1 and Q_2. However, when the excitation was large enough that no real solution of Eq. (154) could be obtained, the zero mean model characterized by the variance of Eq. (156) was used. The results of Fig. 3.1 clearly demonstrate that the combination of the two nonzero mean solutions yields an extremely accurate estimate of the overall standard deviation but that its zero mean counterpart (for $SPL \geq 120$ dB) can severely underestimate this moment although the accuracy appears to be improving as the sound pressure level increases past the fluctuation to snap-through transition region. Figure 3.1 also demonstrates that the second equivalent linearization strategy is not as reliable as the first one except for $SPL \geq 120$ dB. In fact, it exhibits the wrong trend in the low sound pressure level regime, the estimated standard deviation increases as a function of the SPL. This undesirable property is associated with the fixed value of the means $\mu_i = Q_i$ which does not allow the good modeling of the unsymmetry of the local stiffness discussed above. On the basis of these results, it is suggested to use the equivalent linearization strategy #1 when nonzero means exist and to rely the second strategy when such solutions are not possible. The above trends occur consistently through the investigated range of temperatures $s \in [1, 5]$.

It should further be noted from Fig. 3.1 that the average of the standard deviation estimates corresponding to the equivalent linearization strategies 1 and 2 approximates in fact remarkably well its exact counterpart for $SPL \geq 120$. A similar accuracy has also been observed at other values of the temperature s indicating that this averaging could consistently be used to refine the equivalent linearization estimates.

A different perspective on the reliability of the equivalent linearization techniques can be obtained by comparing the produced probability density functions with their exact counterparts. This comparison is presented in Fig. 3.2-3.7. Note first that the improved accuracy of the standard deviation estimate obtained from the equivalent linearization #1 at "low" SPL is obtained by allowing a mean shift of the corresponding distribution. This effect is small but apparent, see Fig. 3.2 for SPL = 114dB and s = 1.8. This shift increases with the sound pressure level and provokes an undesirable error in the prediction of the location of the peaks of the probability density function, see Fig. 3.3 for

SPL = 119dB. The equivalent linearization strategy #2, on the contrary, maintains the location of the peaks at the buckling states as shown in Fig. 3.4 but overestimates the height of the peak. Note also that both methods fail to capture the probability of crossing the origin, i.e. of the occurrence of snap-throughs.

At higher *SPL* still, the equivalent linearization strategy #1 fails to produce a non-zero mean solution resulting in a substantial overshoot of the probability of crossing the origin, see Fig. 3.5. Although the second equivalent linearization approach appears to capture quite well the exact probability density function for this condition, as shown in Fig. 3.6, it also will produce single peak distribution as the sound pressure level continues to increase or equivalently as the temperature decreases, as can be noted from Fig. 3.7.

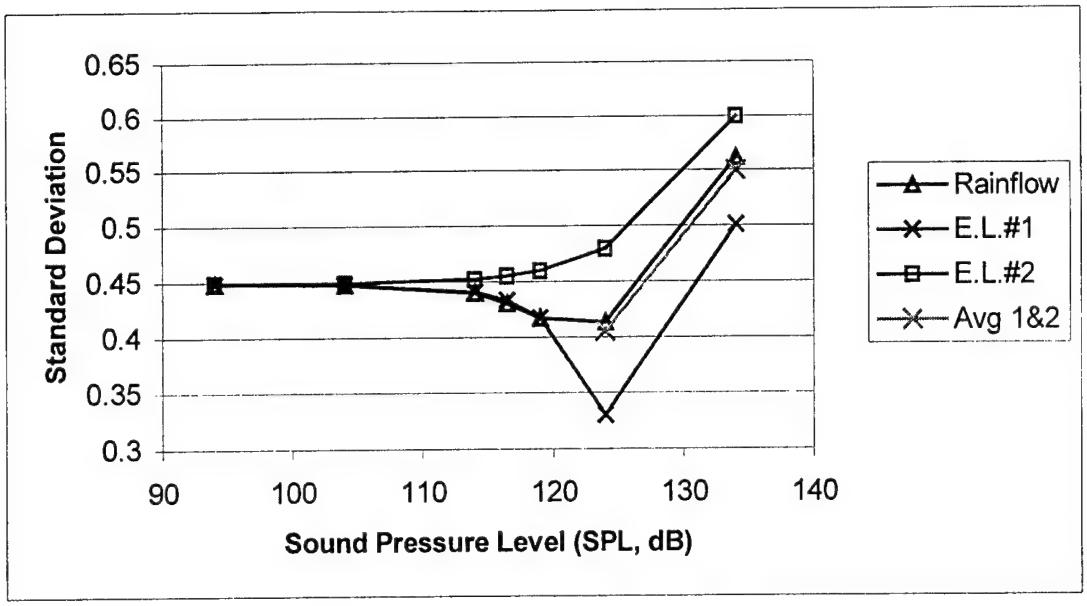

Figure 3.1. Standard deviations of the response as functions of the sound pressure level obtained by simulation and by the equivalent linearization strategies #1 and #2 for $s = 1.8$.

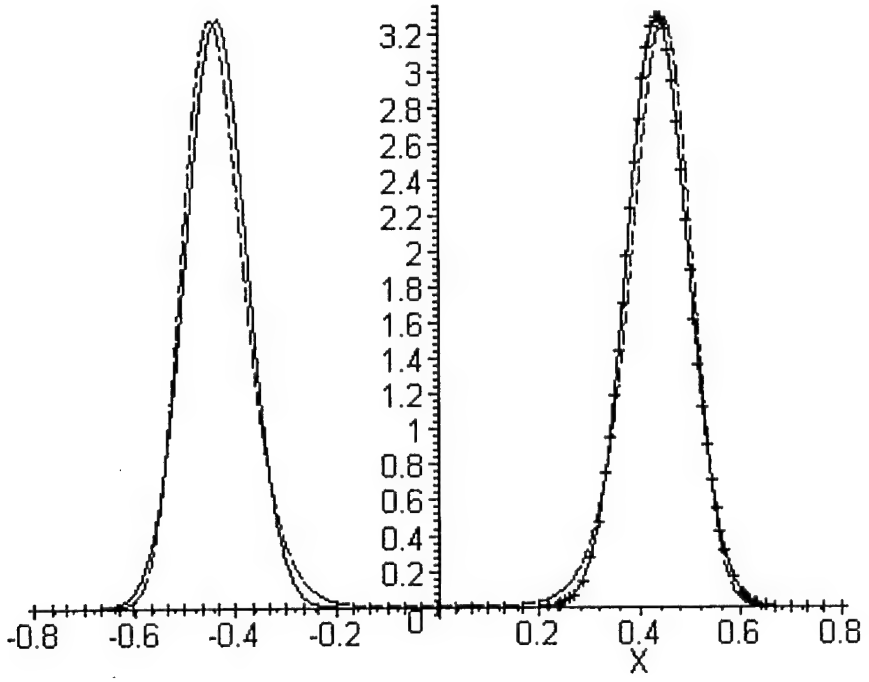

Figure 3.2 Probability density functions of the displacement, exact (---) and estimated according to the equivalent linearization #1 (+++), $s = 1.8$, $SPL = 114$dB.

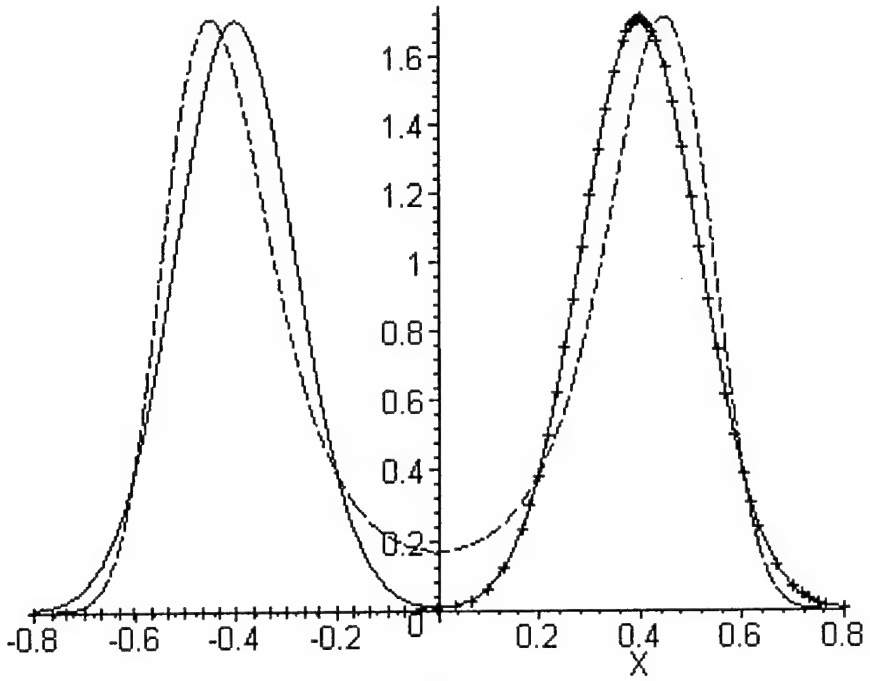

Figure 3.3 Probability density functions of the displacement, exact (---) and estimated according to the equivalent linearization #1 (+++), s = 1.8, SPL = 119dB.

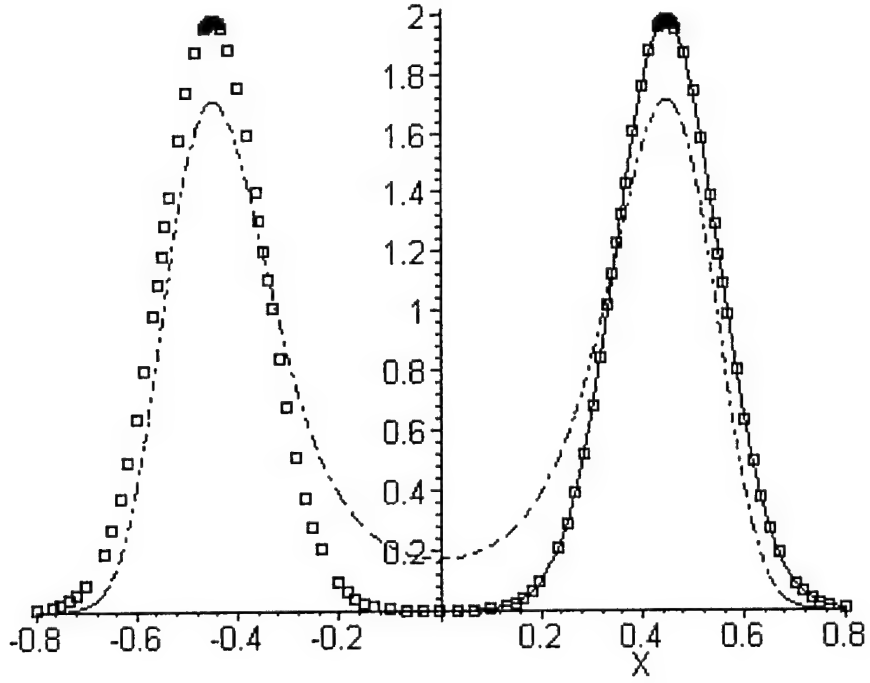

Figure 3.4 Probability density functions of the displacement, exact (---) and estimated according to the equivalent linearization #2 (□□□), s = 1.8, SPL = 119dB.

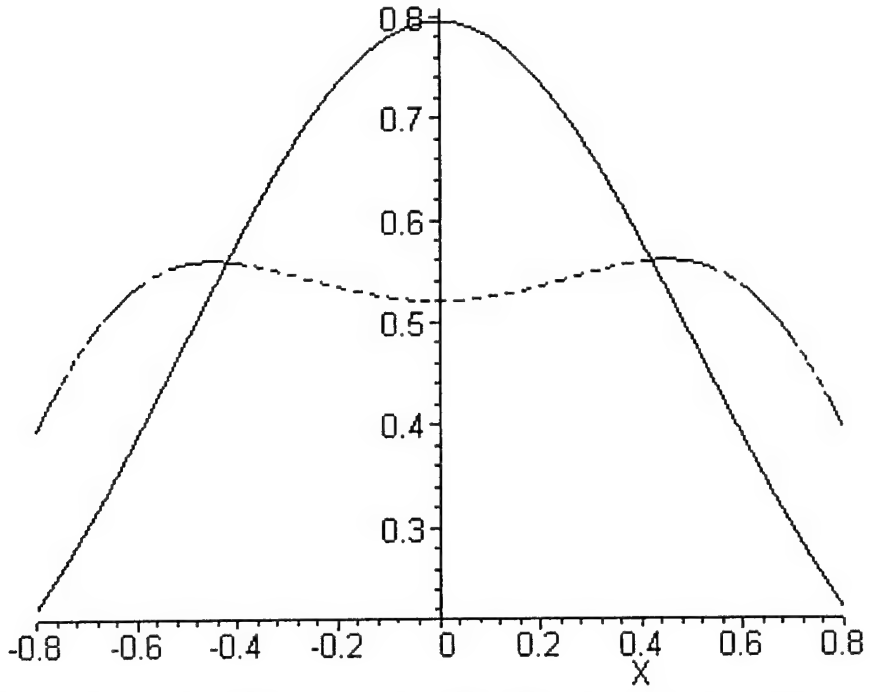

Figure 3.5 Probability density functions of the displacement, exact (---) and estimated according to the equivalent linearization #1 (—), $s = 1.8$, $SPL = 134$dB.

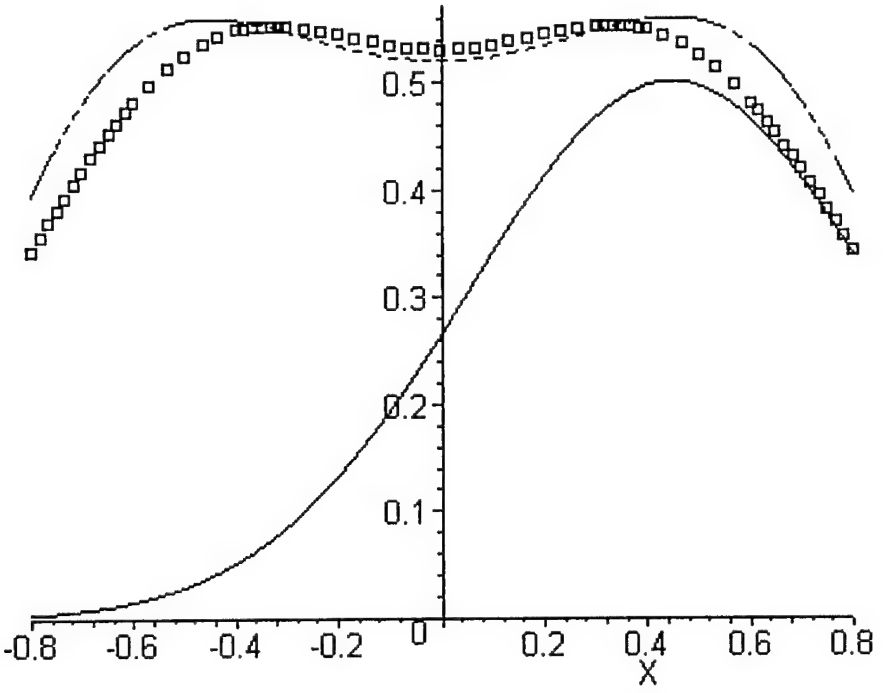

Figure 3.6 Probability density functions of the displacement, exact (---) and estimated according to the equivalent linearization #2: around top buckling state (—) and combined (□□□), $s = 1.8$, $SPL = 134$dB.

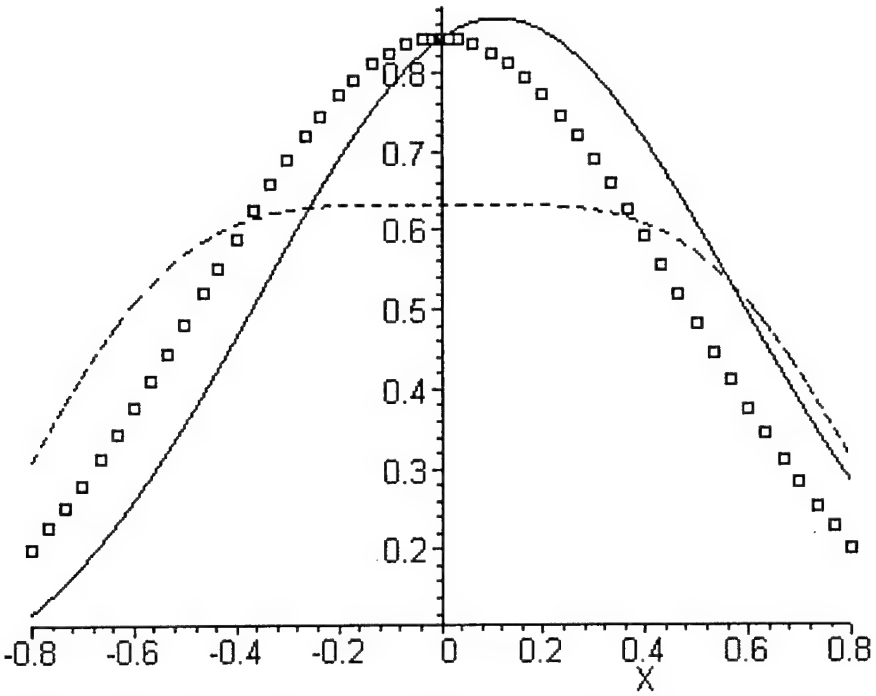

Figure 3.7 Probability density functions of the displacement, exact (---) and estimated according to the equivalent linearization #2: around top buckling state (——) and combined (□□□), $s = 1.05$, $SPL = 134$dB.

SECTION 4
FATIGUE DAMAGE PREDICTION

The second predictive aspect of this investigation focused on the estimation of the accumulated damage by using the equivalent linearization results. That is, it was desired to duplicate at best rainflow results (Downing and Socie, 1982) obtained from the numerically evaluated displacement/stresses time histories from the mean and variances given by Eq. (151), (152), (154)-(156), and (162). To this end, three approaches of increasing complexity were investigated, all of which rely in some fashion on the Rayleigh approximation (see Lutes and Sarkani, 1997) and on an expected narrowbandedness of the response processes (displacement, velocity, stresses, etc.). In assessing the properties of each of these approximations, it should first be noted that the displacement q is not a Gaussian process because of the cubic nonlinearity of Eq. (132) and that the displacement-stress relationship is also nonlinear as seen in Eq. (127). Thus, even if the displacements were Gaussian, the stresses would not. In this light, the three formulations to be presented in sections 4.2-4.4 rely on the following assumptions:

(1) both stresses and displacements are Gaussian ("standard" Rayleigh formulation)

(2) the displacements are Gaussian but the stresses are not, the nonlinear displacement-stress relationship describes the distribution of stresses (nonlinear displacement-stress formulation)

(3) the displacements are specified as the sum of Gaussian-type processes describing the specificities of the fluctuations around the buckled states and the snap-throughs. In this detailed model, the nonlinear displacement-stress relationship describes the distribution of stresses (phenomenological formulation).

Before these three distinct approaches are described, however, an exact formula for the accumulated damage will be presented that was found quite useful in interpreting the numerical results.

4.1 Damage Accumulated: An Exact Formula

In assessing the damage accumulation in the panel, it is first assumed that the material is characterized by the S-N curve

$$N_f = K\, S_r^{-m} \tag{164}$$

where N_f is the number of cycles to failure when the stress range is S_r, and K and m are material constants. Further, adopting a linear damage accumulation rule, the total damage in the panel after a time T_{fin} can be estimated as

$$D\left(T_{fin}\right) = \sum_{k=1}^{n_c\left(T_{fin}\right)} \frac{1}{2\,N_f(k)} = \frac{1}{2\,K} \sum_{k=1}^{n_c\left(T_{fin}\right)} S_{r,k}^{m} \tag{165}$$

where $n_c(T_{fin})$ denotes the total number of half-cycles in the time interval $t \in [0, T_{fin}]$ and $S_{r,k}$ represents the stress range in the k^{th} half-cycle. Note that this quantity can also be represented as

$$S_{r,k} = |S(t_k) - S(t_{k-1})| = \left| \int_{t_{k-1}}^{t_k} \dot{S}(\tau)\, d\tau \right| = \int_{t_{k-1}}^{t_k} |\dot{S}(\tau)|\, d\tau \tag{166}$$

where t_{k-1} and t_k denote the beginning and ending times of the stress range $S_{r,k}$. Further, the last equality in the above relation holds because of the constant sign of the stress velocity $\dot{S}(t)$ in the interval $t \in [t_{k-1}, t_k]$. Combining Eq. (165) and (166) in the special case $m = 1$ yields

$$D(T_{fin}) = \frac{1}{2K} \sum_{k=1}^{n_c(T_{fin})} S_{r,k} = \frac{1}{2K} \sum_{k=1}^{n_c(T_{fin})} \int_{t_{k-1}}^{t_k} |\dot{S}(\tau)|\, d\tau = \frac{1}{2K} \int_0^{T_{fin}} |\dot{S}(\tau)|\, d\tau . \tag{167}$$

Moreover, relying on the stationarity of the stress velocity process, it is found that the expected damage accumulated in the time interval $t \in [0, T_{fin}]$ can be expressed as

$$E[D(T_{fin})] = \frac{1}{2K} \int_0^{T_{fin}} E[|\dot{S}(\tau)|]\, d\tau = \frac{1}{2K} E[|\dot{S}|] \int_0^{T_{fin}} d\tau = \frac{1}{2K} E[|\dot{S}|] T_{fin} . \tag{168}$$

A final simplification of the above relation can be obtained by noting from Eq. (127) that

$$\dot{S} = \dot{q}\,(C_1 + 2\,C_2\,q) \tag{169}$$

where the velocity $\dot{q}$ is known to be Gaussian with mean zero and standard deviation $\sigma_{\dot{q}} = \sqrt{\dfrac{\pi\, S_{pp}}{2\,\xi\,\omega_0}}$ and to be independent of the displacement q (see Lutes and Sarkani, 1997). Then,

$$E[|\dot{S}|] = E[|\dot{q}|]\, E[|C_1 + 2\,C_2\,q|] = \sqrt{\frac{2}{\pi}}\, \sigma_{\dot{q}}\, E[|C_1 + 2\,C_2\,q|] \tag{170}$$

and the expected damage is given by

$$E[D(T_{fin})] = \frac{1}{\sqrt{2\pi}\,K}\, \sigma_{\dot{q}}\, E[|C_1 + 2\,C_2\,q|]\, T_{fin} . \tag{171}$$

A generalization of the above relation for $m \neq 1$ is unfortunately unavailable, even for integer values of m. Indeed, in these cases, an expression for the expected damage in terms of the m point correlation of the stress velocity process can be derived by proceeding as in Eq. (166)-(168). However, the lack of existence of a closed form solution for the transition probability density function of the displacement q and velocity $\dot{q}$ prevents the derivation of a manageable expression for the expected damage. One must then resort to either rainflow simulations or to the use of approximate relations as derived in the next sections.

4.2 Damage Accumulated: "Standard" Rayleigh Formulation

The simplest approximate expression for the accumulated damage used in the present investigation is traditionally referred to as the Rayleigh approximation (see Lutes and Sarkani, 1997). It is derived by assuming that

(i) the stress process $S(t)$ is Gaussian

(ii) the stress process $S(t)$ is narrowband (required unless $m = 1$).

Under these two conditions, it can be shown (see Lutes and Sarkani, 1997) that

$$E\left[D\left(T_{fin}\right)\right]=\frac{1}{2\pi}\,\frac{\sigma_{\dot{S}}}{\sigma_S}\,E[\Delta D]\;T_{fin} \tag{172}$$

where σ_S and $\sigma_{\dot{S}}$ are the standard deviations of the stress and stress velocity processes. Further, $E[\Delta D]$ denotes the expected damage accumulated over one cycle of the stress process which can be estimated as

$$E[\Delta D]=\frac{2^{3m/2}}{K}\,\Gamma\left(1+\frac{m}{2}\right)\sigma_S^m \tag{173}$$

so that

$$E\left[D\left(T_{fin}\right)\right]=\frac{1}{2\pi}\,\frac{2^{3m/2}}{K}\,\Gamma\left(1+\frac{m}{2}\right)\sigma_{\dot{S}}\;\sigma_S^{m-1}\;T_{fin}\,. \tag{174}$$

It is known that the Rayleigh approximation is exact when $m = 1$ under weaker conditions that the two stated above, (i) and (ii). In fact, when $m = 1$, it is only necessary that the stress velocity process be Gaussian. This property can be confirmed by noting that Eq. (174) reduces to Eq. (171) when $m = 1$ and $C_2 = 0$.

The determination of the standard deviations σ_S and $\sigma_{\dot{S}}$ can be accomplished from Eq. (127) and (169). Specifically, relying on the Gaussian character of q and $\dot{q}$, it is found that

$$\sigma_S^2 = C_1^2\;\sigma_q^2 + C_2^2\left(4\,\mu_q^2 + 2\,\sigma_q^2\right)\sigma_q^2 + 4\,C_1\,C_2\,\mu_q\,\sigma_q^2 \tag{175}$$

and

$$\sigma_{\dot{S}}^2 = \sigma_{\dot{q}}^2\left[C_1^2 + 4\,C_2^2\left(\mu_q^2 + \sigma_q^2\right) + 4\,C_1\,C_2\,\mu_q\right]\,. \tag{176}$$

It should be noted that this formulation is simple but it is also inconsistent: it assumes that both the stresses and displacements are Gaussian and, at the same time, that they are nonlinearly related through Eq. (127) and (169).

4.3 Damage Accumulated: Nonlinear Displacement-Stress Formulation

The removal of the inconsistency of the Rayleigh formulation described above can be accomplished by formulating the entire problem in terms of the displacement q which here will be assumed to be a Gaussian process (or a combination thereof). The approach presented below follows the non-Gaussian correction scheme introduced by Lutes and Sarkani (1997). For clarity of the presentation, assume momentarily that the displacement-stress relationship $S = g(q)$ is monotonic (this is clearly not always the case for Eq. (127)) and that the response processes are narrowband. Then, it can be

argued that the positive (S^+) and negative (S^-) peak stresses of a given stress range correspond to peak values of the displacement q. Further, under the narrowbandedness assumption, the peak deviations from the mean displacement follow a Rayleigh distribution and the positive and negative maximum deviations of a given cycle are approximately equal. That is,

$$S^+ = g\left(\mu_q + \sigma_q\, u\right) \qquad \text{and} \qquad S^- = g\left(\mu_q - \sigma_q\, u\right) \tag{177}$$

where u is a standard Rayleigh random variable. Accordingly, the expected damage accumulated over a cycle is

$$E[\Delta D] = \frac{1}{K} E\left[\left| S^+ - S^- \right|^m\right] = \frac{1}{K} \int_0^\infty \left[\left| g\left(\mu_q + \sigma_q\, u\right) - g\left(\mu_q - \sigma_q\, u\right)\right|^m\right] u \exp\left(-u^2/2\right) du \tag{178}$$

Equation (178) is not directly applicable here since Eq. (127) is not monotonic. Indeed, there exists an extremum (minimum or maximum) of the stress for $q = q_e = -\dfrac{C_1}{2\,C_2}$ and the corresponding stress is $S_e = C_0 - \dfrac{C_1^2}{4\,C_2}$. On physical grounds, it is expected here that the membrane stresses yield a stretching effect so that $C_2 \geq 0$ and the extremum is always a minimum. Thus, for all values of $u \geq u_e = \left| q_e - \mu_q \right| / \sigma_q$, the stress process does not undergo a single cycle of magnitude $\left| S^+ - S^- \right|$ but rather two separate cycles of respective amplitudes $\left| S^+ - S_e \right|$ and $\left| S_e - S^- \right| = \left| S^- - S_e \right|$. Accordingly, the expected damage accumulated over the cycle of *displacement* is

$$E[\Delta D] = \frac{1}{K} \int_0^{u_e} \left[\left| g\left(\mu_q + \sigma_q\, u\right) - g\left(\mu_q - \sigma_q\, u\right)\right|^m\right] u \exp\left(-u^2/2\right) du$$
$$+ \frac{1}{K} \int_{u_e}^\infty \left[\left| g\left(\mu_q + \sigma_q\, u\right) - S_e \right|^m + \left| g\left(\mu_q - \sigma_q\, u\right) - S_e \right|^m\right] u \exp\left(-u^2/2\right) du \tag{179}$$

where

$$S = g(q) = C_0 + C_1\, q + C_2\, q^2. \tag{180}$$

Finally, relying on the expected narrowband character of the displacement process and the assumed Gaussian distribution of the displacement and velocity processes, the period can be estimated through the expected rate of upcrossing of the mean value as $T = \dfrac{2\pi\,\sigma_q}{\sigma_{\dot{q}}}$ so that the expected damage accumulated in the time interval $t \in [0, T_{fin}]$ is given as

$$E\left[D\left(T_{fin}\right)\right] = \left[\frac{1}{2\pi}\frac{\sigma_{\dot{q}}}{\sigma_q}\right] E[\Delta D]\; T_{fin}. \tag{181}$$

For example, for $m = 1$, Eq. (179) becomes

$$E[\Delta D] = \frac{2}{K}(C_0' - S_e)\exp\left(-\frac{u_e^2}{2\sigma_q^2}\right) + \frac{2}{K}C_1'\left[-|u_e|\exp\left(-\frac{u_e^2}{2\sigma_q^2}\right) + \sigma_q\,\Phi\left(\frac{|u_e|}{\sigma_q}\right)\right]$$
$$+\frac{4}{K}C_2'\,\sigma_q^2\left(1+\frac{u_e^2}{2\sigma_q^2}\right)\exp\left(-\frac{u_e^2}{2\sigma_q^2}\right) \qquad (182)$$

where

$$C_0' = C_0 + C_1\,\mu_q + C_2\,\mu_q^2; \quad C_1' = C_1 + 2C_2\,\mu_q; \quad C_2' = C_2 \qquad (183a\text{-}c)$$

and

$$\Phi(x) = \int_0^x \exp\left(-\frac{u^2}{2}\right)du\,. \qquad (184)$$

As a check, consider the case $C_2 = 0$ for which $q_e = \infty$ so that Eq. (182) reduces to $E[\Delta D] = C_1\sqrt{2\pi}\,\frac{\sigma_q}{K}$ and $E\left[D\left(T_{fin}\right)\right] = \frac{1}{\sqrt{2\pi}}\frac{C_1}{K}\sigma_{\dot{q}}\;T_{fin}$ as expected from Eq. (171).

The case $C_1 = 0$, $\mu_q = 0$ is also very important as it corresponds to the most strongly nonlinear displacement-stress relationship and thus represents a good test of this second damage accumulation formulation. Accordingly, it is found that $q_e = 0$ and $S_e = 0$ so that

$$E[\Delta D] = \frac{4}{K}C_2\,\sigma_q^2 \qquad \text{and} \qquad E\left[D\left(T_{fin}\right)\right] = \frac{2}{\pi}\frac{C_2}{K}\sigma_{\dot{q}}\,\sigma_q\,T_{fin} \qquad (185a,b)$$

4.4 Damage Accumulated: Phenomenological Formulation

The nonlinear displacement-stress formulation presented in the last section accounted fully and exactly for the nonlinear q to S transformation so that improvements over this strategy require the consideration of non-Gaussian displacements. In keeping with the stated goals of this investigation to obtain an estimation strategy of the damage accumulated that can be extended to multi-modes, it is proposed here to introduce a formulation based on a "combination" of Gaussian processes that is valid for panels statically buckled, i.e. for $s > 1$. Specifically, in accord with the non-zero mean equivalent linearization strategies developed above, it will be assumed that the motion around each buckled configuration follows a Gaussian distribution so that the probability density function of q is the weighted sum of two Gaussian distributions of means exactly or approximately equal to the buckled states. That is,

$$p_{q(t)}(q) = q_1\frac{1}{\sqrt{2\pi}\,\sigma_1}\exp\left(-\frac{(q-\mu_1)^2}{2\sigma_1^2}\right) + q_2\frac{1}{\sqrt{2\pi}\,\sigma_2}\exp\left(-\frac{(q-\mu_2)^2}{2\sigma_2^2}\right) \qquad (186)$$

where the probabilities (weights) q_1 and q_2 are selected so that

$$q_1 + q_2 = 1 \qquad \text{and} \qquad \omega_0^2\,(1-s)\,E[q] + \gamma\,E\left[q^3\right] = \bar{p}_0\,, \qquad (187a,b)$$

i.e., so that q has a total probability of 1 and that Eq. (132) is satisfied at least on average. In particular when $\bar{p}_0 = 0$, it is directly found that $q_1 = q_2 = 1/2$ as expected. Note in Eq. (186) that the means μ_1, μ_2 and standard deviations σ_1, σ_2 can be estimated from the equivalent linearization #1 (provided solutions μ_1, μ_2 to Eq. (151) exist) or #2.

Once the probability density function of q, Eq. (186), is known, it is necessary to evaluate the damage accumulated. To this end, it is suggested here to investigate separately the fluctuations around each buckled configurations and the snap-throughs from one such position to the other. Both fluctuation and jump processes will be considered to be narrowband so that their corresponding damages can accurately be estimated by Rayleigh's formula,

$$E\left[D\left(T_{fin}\right)\right] = n\, E[\Delta D] \tag{188}$$

where n is the expected number of cycles occurring in the time interval of length T_{fin}. To exemplify the determination of the damage per cycle, $E[\Delta D]$, and the number of cycles n, consider a half-cycle of motion with $q(t_{k-1}) \geq q(t_k)$ and note that there are three distinct possibilities for the displacement time history, i.e.

(a) fluctuation around the top buckled state
(b) snap-through from top to bottom buckled state
(c) fluctuation around the bottom buckled state

as depicted in Fig. 4.1. To evaluate the likelihood of each of these three trajectories, it is first necessary to estimate the probabilities p_1 and p_2 that the peak displacement $q(t_{k-1})$ is around the top and bottom buckled states, respectively. To this end, assume for simplicity that $\bar{p}_0 = 0$ and introduce the probability of snap-through p so that the probabilities of the trajectories (a)-(c) are

$$p_a = p_1\,(1-p) \qquad p_b = p_1\, p \qquad \text{and} \qquad p_c = p_2\,. \tag{189a-c}$$

Accordingly, the probability that the valley of the half-cycle be located near the bottom buckled state is $p_b + p_c$ which should also equal to p_1 since the displacement process q is symmetric when $\bar{p}_0 = 0$. It is then required that

$$p_b + p_c = p_1\, p + p_2 = p_1\,. \tag{190}$$

Since the total probability for the peak location must equal 1, one also has the condition

$$p_1 + p_2 = 1 \tag{191}$$

and the solution of Eq. (190) and (191) yields

$$p_1 = \frac{1}{2-p} \qquad \text{and} \qquad p_2 = \frac{1-p}{2-p}\,. \tag{192a,b}$$

In fact, the peak to valley transition process has been represented as a Markov chain with a transition probability p which need now be evaluated. This determination requires a physical characterization of the occurrence of snap-throughs. To this end, note that snap-throughs are associated with the existence of a softening region, see Fig. 4.2, in which the local stiffness is negative. The domain of attraction around one of the buckling states could be defined as the region in which the potential is less than or equal to the value at $q = 0$. The values Q_{1T} and Q_{2T} bounding this region are then such that

$$\frac{1}{2}\omega_0^2\,(1-s)\,Q_{iT}^2+\frac{1}{4}\gamma\,Q_{iT}^4=0 \tag{193}$$

from which it is found that

$$Q_{iT}=\pm\sqrt{-\frac{2\,\omega_0^2\,(1-s)}{\gamma}}\ . \tag{194}$$

Then, it is suggested that a snap-through occurs, i.e. trajectory (a) turns into (b), when the extreme displacement corresponding to the valley of the half-cycle, $q(t_k)$, falls outside of the domain of attraction, i.e.

$$p=\Pr\left[q(t_k)>Q_{1T}\right]=\exp\left[-\frac{(Q_{1T}-\mu_1)^2}{2\,\sigma_1^2}\right] \tag{195}$$

where the last equality holds in view of the expected Rayleigh distribution of the peak displacement values $q(t_k)$.

The combination of Eq. (192) and (195) yields the probabilities associated with the three possible trajectories (a)-(c). Further, the corresponding damage contributions $E[\Delta D_a]$, $E[\Delta D_b]$, and $E[\Delta D_c]$ can be evaluated as in Eq. (179), (180), and (182) so that the total damage can be evaluated as

$$E\left[D\left(T_{fin}\right)\right]=n_a\;E[\Delta D_a]+n_b\;E[\Delta D_b]+n_c\;E[\Delta D_c] \tag{196}$$

where n_a, n_b, and n_c are the number of cycles corresponding to each type of trajectory (a)-(c). These values can be expected to be proportional to the probability of occurrence of their corresponding trajectory, Eq. (189), that is

$$n_a=p_1\,(1-p)\,N \qquad n_b=p_1\,p\,N \quad \text{and} \quad n_c=p_2\,N \tag{197}$$

where N denotes the total number of cycles. In turn, this quantity can be estimated from the total time T_{fin} as

$$\frac{n_a}{\nu_a}+\frac{n_b}{\nu_b}+\frac{n_c}{\nu_c}=T_{fin} \tag{198}$$

where the upcrossing rates ν_a, ν_b, and ν_c are estimates of the frequencies of the narrowband trajectories (a)-(c). The Gaussian character of the motions around the buckled states suggests that

$$\nu_a=\frac{1}{2\,\pi}\,\frac{\sigma_{\dot{q}_1}}{\sigma_1} \qquad \text{and} \qquad \nu_c=\frac{1}{2\,\pi}\,\frac{\sigma_{\dot{q}_2}}{\sigma_2} \tag{199a,b}$$

where $\sigma_{\dot{q}_1}$ and $\sigma_{\dot{q}_2}$ are the standard deviations of the velocities associated with the fluctuations around the top and bottom buckled states and can be determined from either equivalent linearization #1 (provided solutions μ_1, μ_2 to Eq. (151) exist) or #2. In fact, they are both equal to the exact expression $\sigma_{\dot{q}}=\sqrt{\dfrac{\pi\,S_{pp}}{2\,\xi\,\omega_0}}$.

The determination of ν_b proceeds similarly but in connection with the overall probability density function of the displacements, i.e. Eq. (186). Specifically, the

upcrossing rate of the undeformed panel configuration, $q = 0$, is given in terms of the joint probability density function of q and $\dot{q}$ as (see Lutes and Sarkani, 1997)

$$\nu_b = \nu_0^+ = \int_0^\infty v\, p_{q\dot{q}}(0, v)\, dv. \tag{200}$$

Assuming that the displacement q and velocity $\dot{q}$ are statistically independent and that the latter random variable is Gaussian, it is found that

$$\nu_b = \nu_0^+ = p_q(0)\frac{\sigma_{\dot{q}}}{\sqrt{2\pi}} \tag{201}$$

where $p_q(0)$ is given by Eq. (186) for $q = 0$. Note the assumptions stated above are not particularly restrictive since they are known to hold for the processes satisfying either the exact equation of motion, Eq. (132), or any of its equivalent linearization approximations.

Combining Eq. (197)-(199) and (201) yields estimates of the number of cycles n_a, n_b, and n_c corresponding to each type of trajectory (a)-(c) and completes the damage accumulation formulation.

4.5 Numerical Results

To establish baseline values the accumulated damages, the numerical integration of the equation of motion (132) was performed as discussed in section 2. From the time histories of the displacement, the corresponding realizations of the stress(es) were obtained through the quadratic relation, Eq. (127). Then, the rainflow cycle counting strategy of (Downing and Socie, 1982) was used to identify stress ranges and evaluate the accumulated damage over a fixed interval of T_{fin} = 32,000 time steps. In keeping with the dimensionless formulation of the equation of motion, the damage was normalized according to $\overline{D} = K\left(\frac{b^2}{E_{eq}\,\pi^2\,h^2}\right)^m D$. Finally, the values of the damage presented in these figures are in fact averages over 100 realizations of stress time histories to reduce the variability of the damage estimates. These 100 simulations were divided into two groups of 50 each with the excitation records in the second set equal in magnitude but of opposite sign to their counterparts in the first set. This procedure was required to ensure that exactly half of the simulations at low sound pressure levels would lead to fluctuations around the upper buckling position with the remaining half around the lower one.

Shown in Fig. 4.3-4.10, are the normalized damages computed on the basis of the stress σ_x at the middle of either the top surface of the panel (Z = 0.5) or its neutral plane (Z = 0). Physically, it can be seen that this stress component is dominated, when Z = 0.5, by the linear bending terms, $C_1\, q$, which is completely absent when Z = 0. Accordingly, it can be expected that this latter situation provides a worst case scenario from the standpoint of nonlinearity of the displacement-stress relations.

Turning now to the prediction approaches, the equivalent linearization strategy #1 was used to provide the estimate of the standard deviation of the displacement process required by the "standard" Rayleigh and nonlinear displacement-stress formulations. On

the contrary, the phenomenological approach relied on the results of the second equivalent linearization strategy, consistently with the basis of this numerical technique. An analysis of these results demonstrates that both the Rayleigh and nonlinear displacement-stress formulations yield reliable estimates of the accumulated damage at "low" sound pressure levels, i.e. when snap-throughs are rare events. These estimates were obtained by averaging the damages corresponding to each of the two nonzero mean models. In effect, this procedure fully accounts for the fluctuation processes but neglects the damage associated with the infrequent snap-throughs.

As the *SPL* approaches the threshold above which the equivalent linearization strategy #1 fails to yield a nonzero mean, snap-throughs are becoming more frequent and both the Rayleigh and nonlinear displacement-stress formulations underestimate the actual damage. In this condition, the phenomenological formulation provides very reliable approximation of the accumulated damage provided that the value of the probability density function $p_q(0)$, governing the rate of snap-throughs, is accurate.

Finally, at high sound pressure levels, i.e. higher than the above threshold, it was found that the Rayleigh approach typically overestimated the exact accumulated damage and that the nonlinear displacement-stress formulation underestimated this value. However, the average of these two estimates (shown in Fig. 4.3-4.10 as "Final") has consistently been found to be an accurate approximation of the damage.

In view of the above results and comments, it is suggested that the nonlinear displacement-stress formulation be used until the sound pressure level approaches the threshold at which the equivalent linearization method #1 stops yielding nonzero mean solutions. Then, in a small region below this value, the phenomenological formulation should be used with an accurate estimate of $p_q(0)$. Finally, above the threshold, the approximate accumulated damage should be obtained as the average of the estimates provided by the Rayleigh and nonlinear displacement-stress formulations.

The above discussions have focused on the prediction of the accumulated damage associated with a specific stress component. In general however, the panel experiences a multiaxial state of stress and it is necessary to define an appropriate equivalent stress. Adopting a Tresca-type failure criterion, it is suggested here to compute the damages associated with the stress components σ_x, σ_y, and $\sigma_x - \sigma_y$. The accumulated damage will then be selected as the largest of these three values. This process is demonstrated in Fig. 4.13-4.15 in connection to a composite panel similar to the one introduced by Kavallieratos (1992) and discussed in Section 2 but with dimensions $a = b = 8$ in. and different lay-ups. The damages shown in Fig. 4.13-4.15 correspond to the point at the middle of the panel on its top surface (Z=0.5).

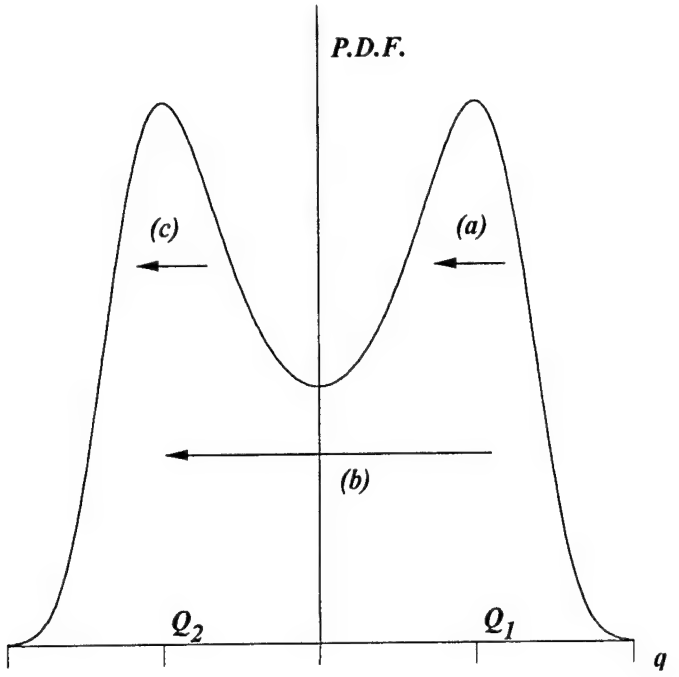

Figure 4.1 Probability density function of the displacement showing the three peak to valley trajectories (a)-(c).

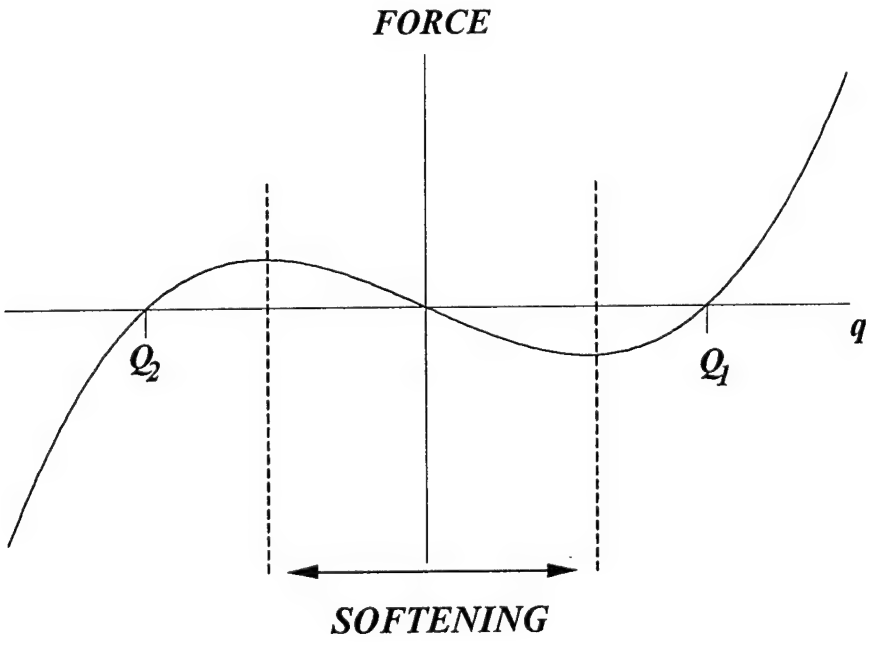

Figure 4.2 Force vs. displacement curve showing the softening region.

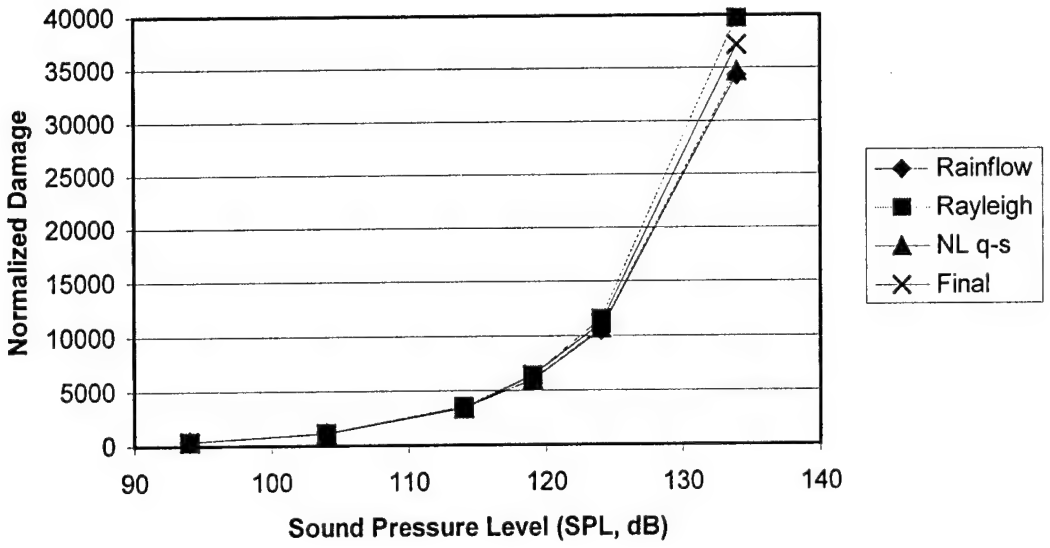

Figure 4.3 Estimates of the nomalized damage as functions of the sound pressure level obtained by rainflow analysis and by the various approximate methods for $m = 1$, $s = 1.8$, $Z = 0.5$.

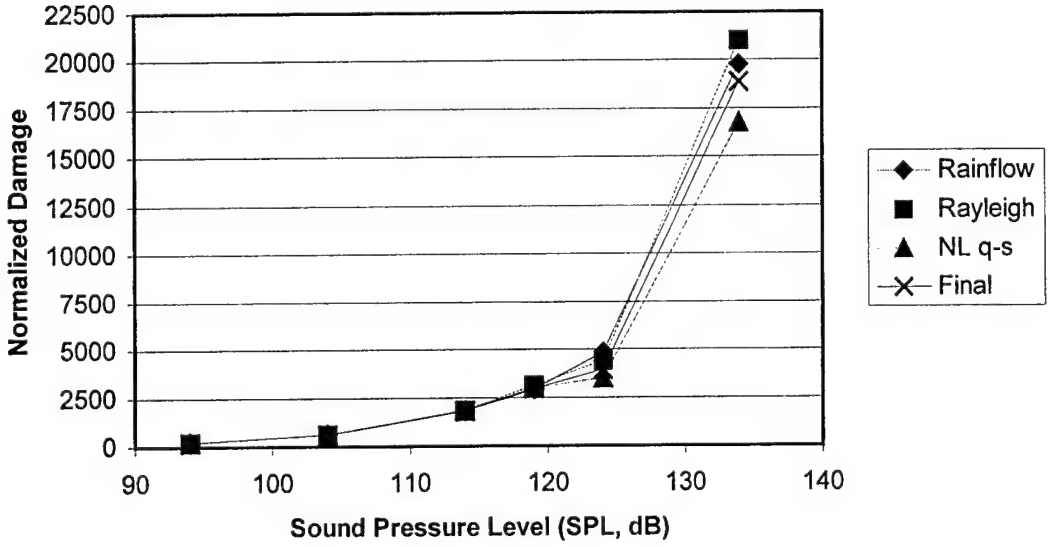

Figure 4.4 Estimates of the nomalized damage as functions of the sound pressure level obtained by rainflow analysis and by the various approximate methods for $m = 1$, $s = 1.8$, $Z = 0$.

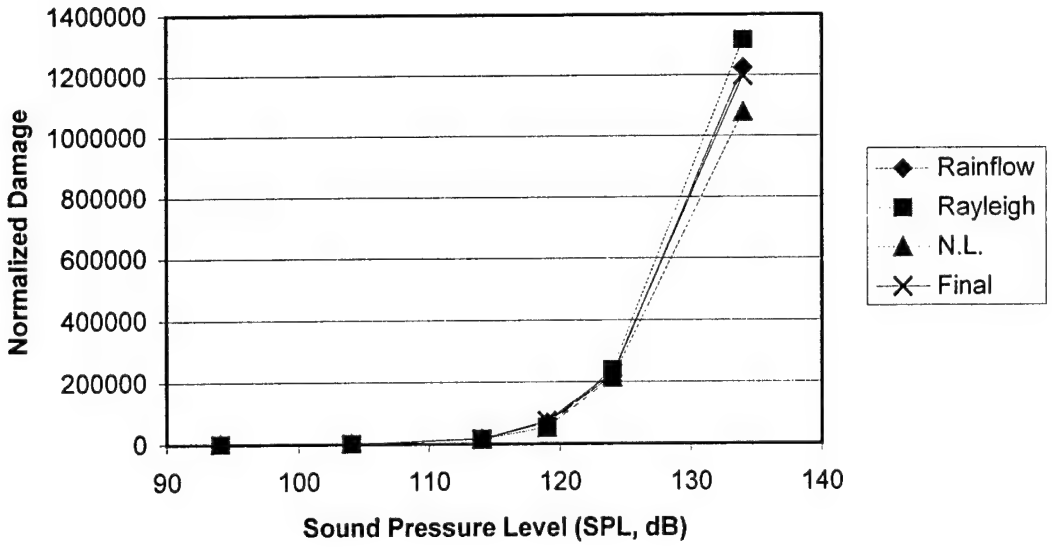

Figure 4.5 Estimates of the nomalized damage as functions of the sound pressure level obtained by rainflow analysis and by the various approximate methods for $m = 2$, $s = 1.8$, $Z = 0.5$.

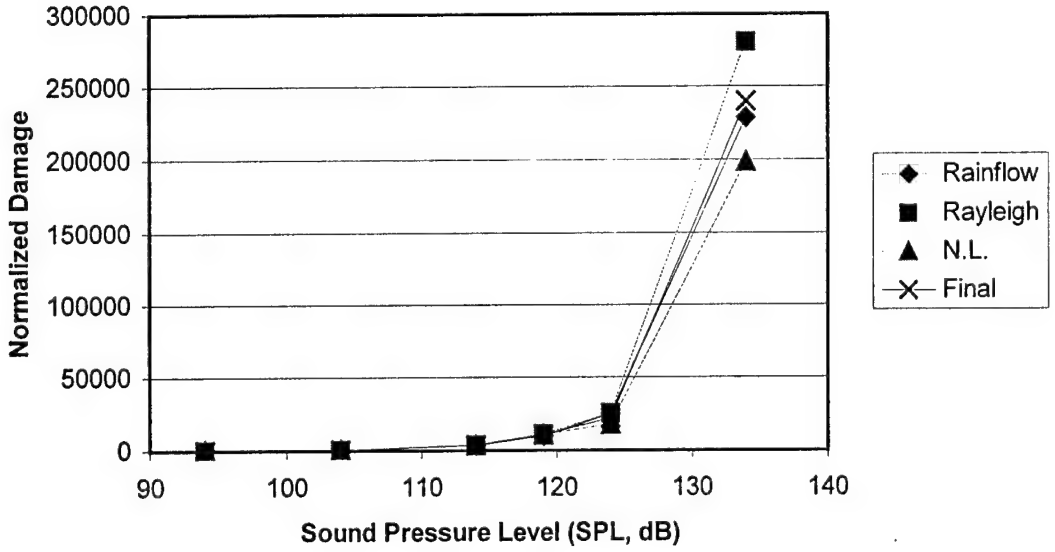

Figure 4.6 Estimates of the nomalized damage as functions of the sound pressure level obtained by rainflow analysis and by the various approximate methods for $m = 2$, $s = 1.8$, $Z = 0$.

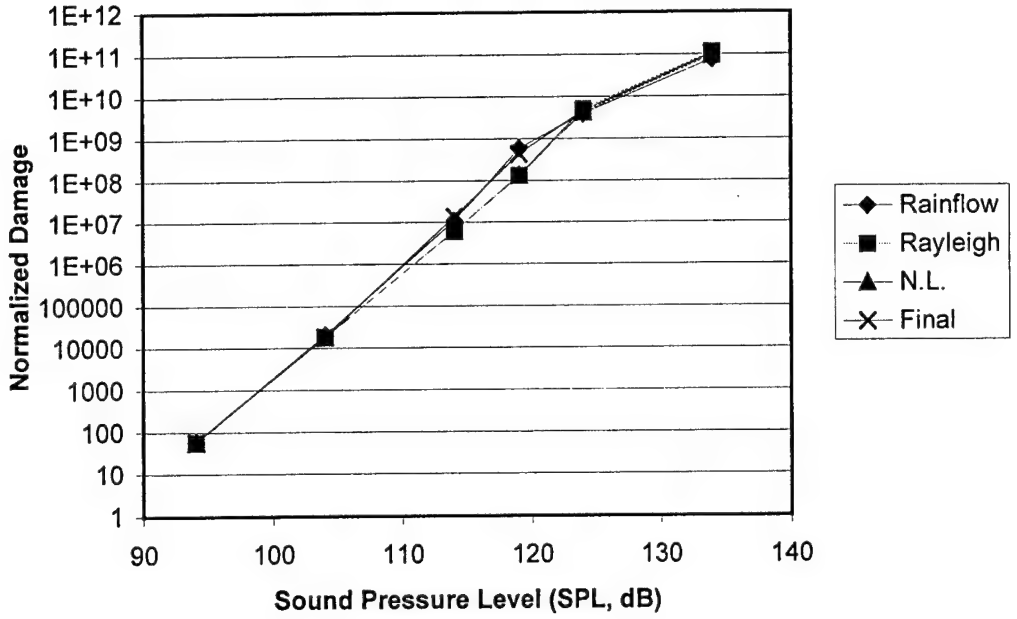

Figure 4.7 Estimates of the nomalized damage as functions of the sound pressure level obtained by rainflow analysis and by the various approximate methods for $m = 5$, $s = 1.8$, $Z = 0.5$.

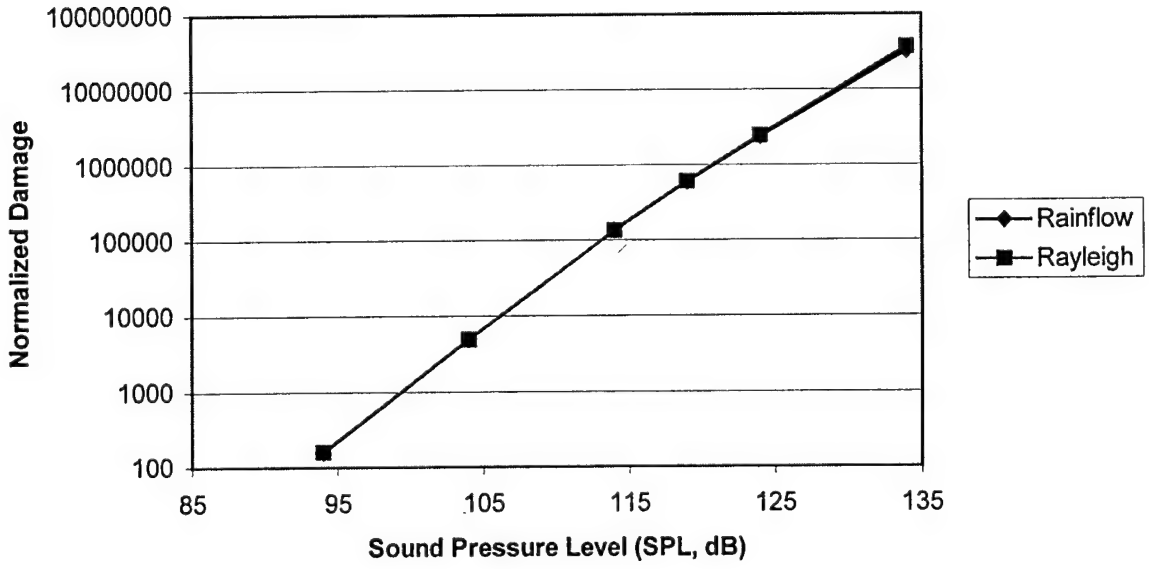

Figure 4.8 Estimates of the nomalized damage as functions of the sound pressure level obtained by rainflow analysis and by the various approximate methods for $m = 3$, $s = 0.5$, $Z = 0.5$.

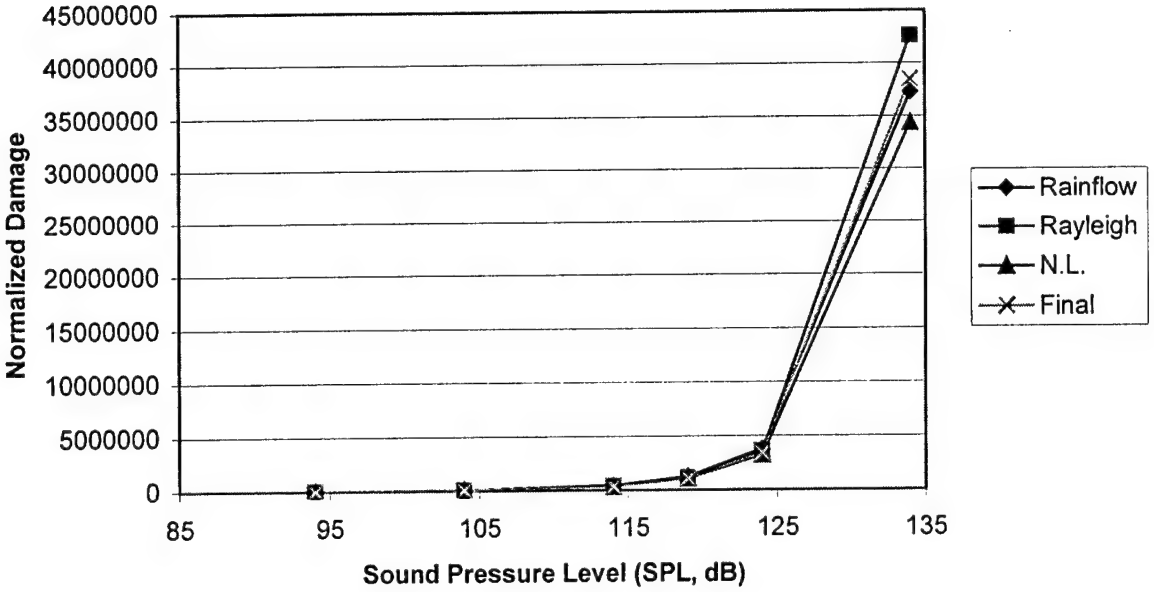

Figure 4.9 Estimates of the nomalized damage as functions of the sound pressure level obtained by rainflow analysis and by the various approximate methods for $m = 3$, $s = 1.05$, $Z = 0.5$.

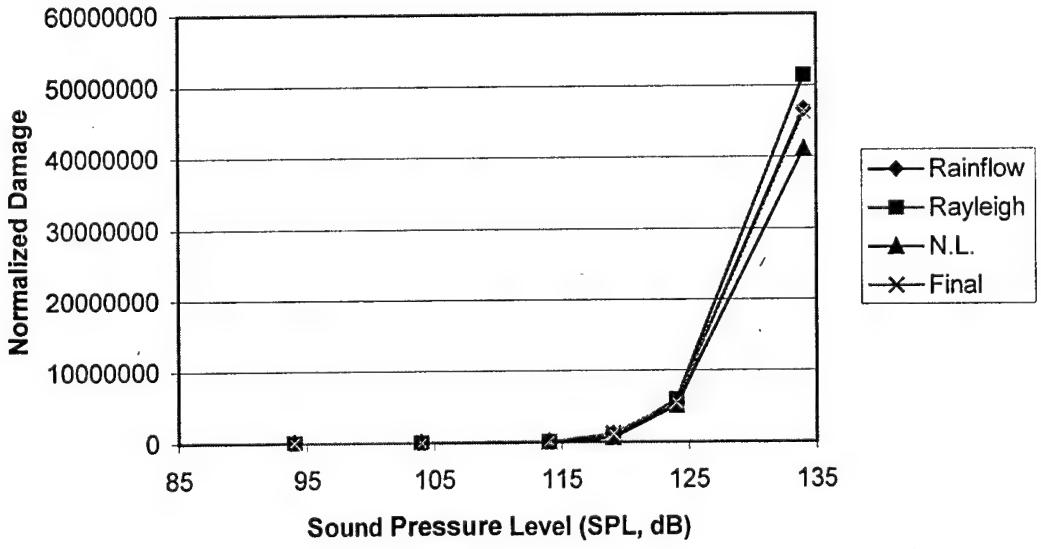

Figure 4.10 Estimates of the nomalized damage as functions of the sound pressure level obtained by rainflow analysis and by the various approximate methods for $m = 3$, $s = 1.8$, $Z = 0.5$.

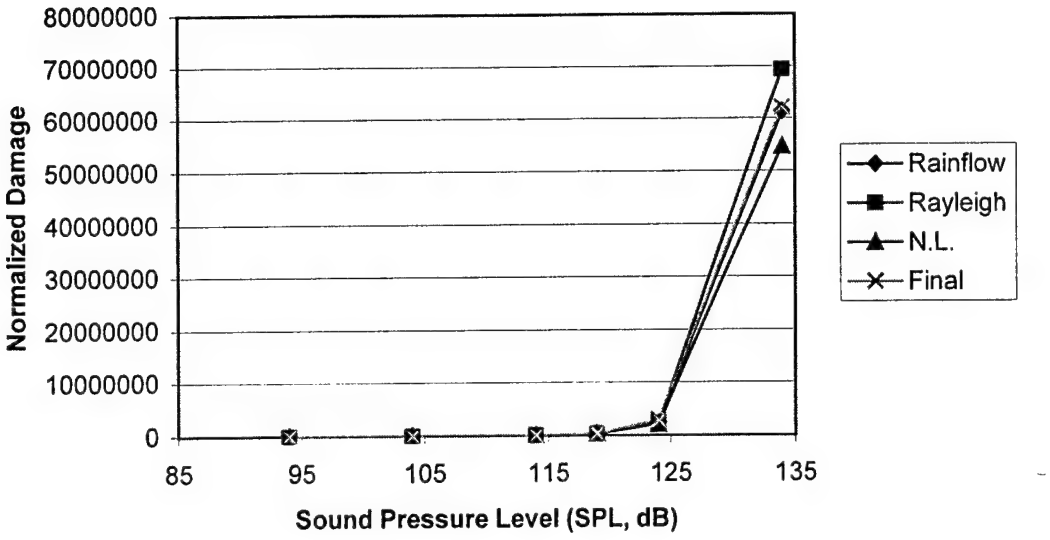

Figure 4.11 Estimates of the nomalized damage as functions of the sound pressure level obtained by rainflow analysis and by the various approximate methods for $m = 3$, $s = 3$, $Z = 0.5$.

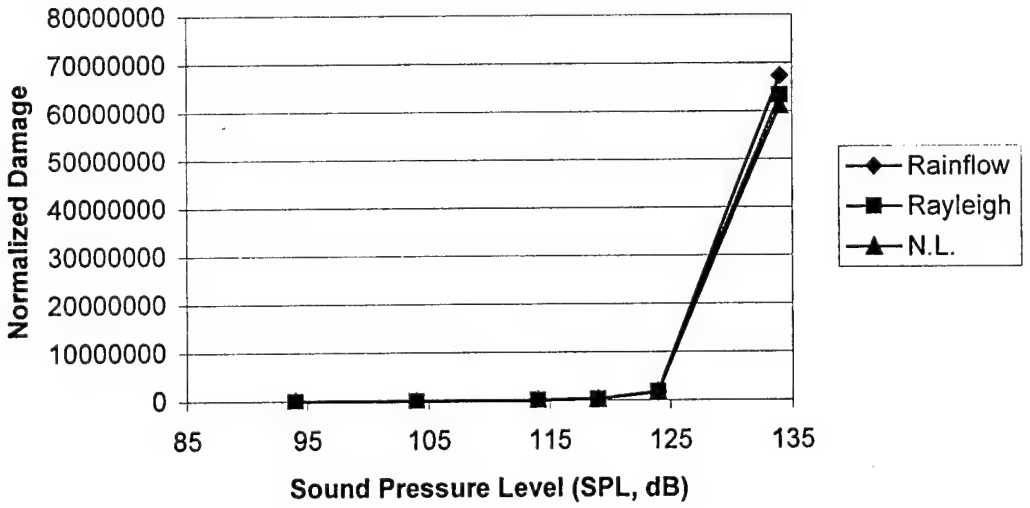

Figure 4.12 Estimates of the nomalized damage as functions of the sound pressure level obtained by rainflow analysis and by the various approximate methods for $m = 3$, $s = 5$, $Z = 0.5$.

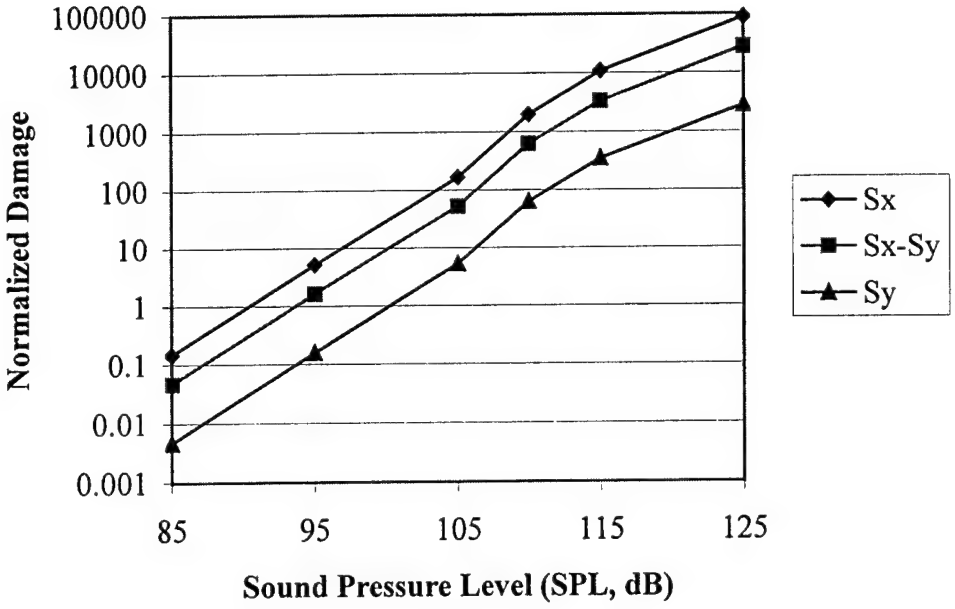

Figure 4.13 Estimates of the nomalized damage as functions of the sound pressure level obtained by rainflow analysis for the lay-up $[90\ 45\ -45\ 0]_s$ with $m = 3$, $s = 1.8$, $Z = 0.5$ and for the stresses σ_x (Sx), σ_y (Sy), and $\sigma_x - \sigma_y$ (Sx - Sy).

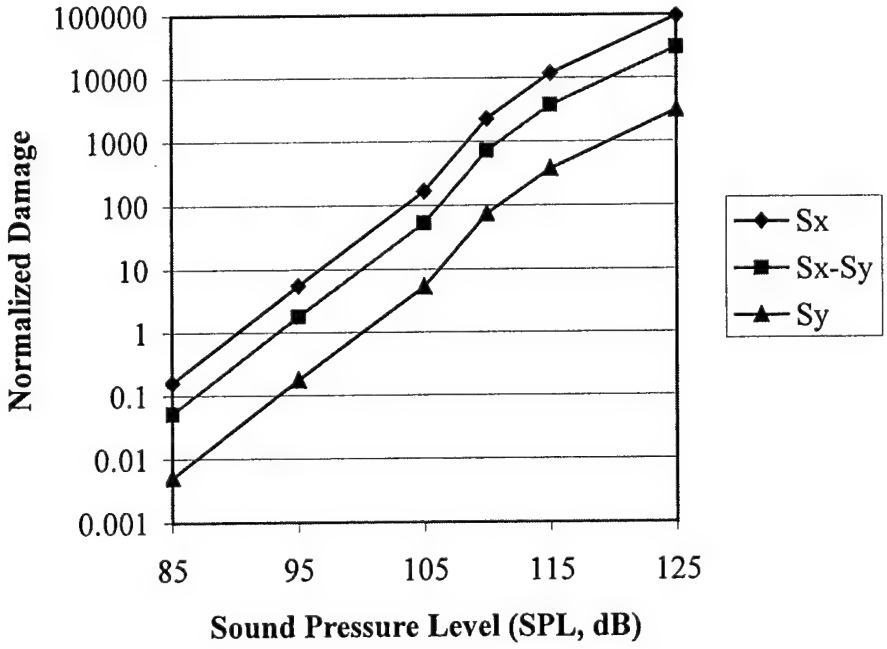

Figure 4.14 Estimates of the nomalized damage as functions of the sound pressure level obtained by rainflow analysis for the lay-up $[-45\ 90\ 45\ 0]_s$ with $m = 3$, $s = 1.8$, $Z = 0.5$ and for the stresses σ_x (Sx), σ_y (Sy), and $\sigma_x - \sigma_y$ (Sx - Sy).

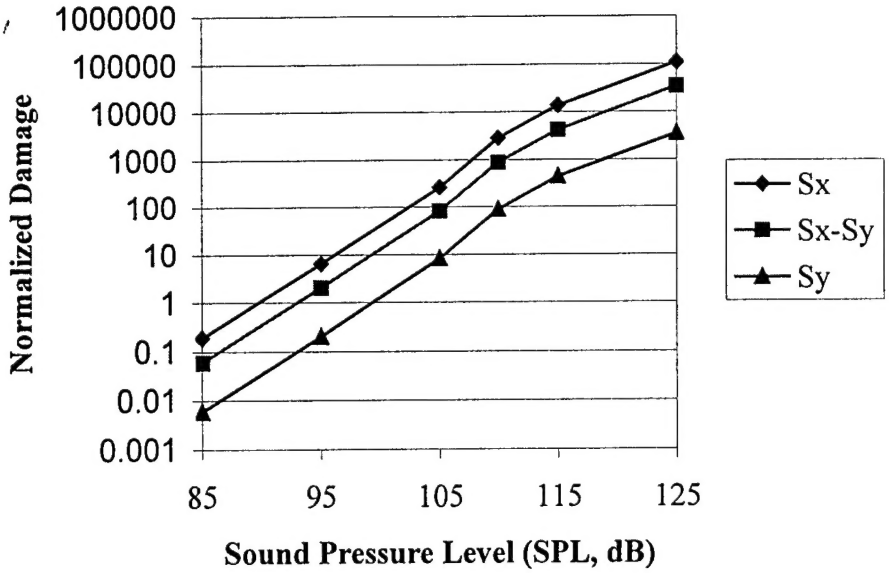

Figure 4.15 Estimates of the nomalized damage as functions of the sound pressure level obtained by rainflow analysis for the lay-up $[45\ -45\ 90\ 0]_s$ with $m = 3$, $s = 1.8$, $Z = 0.5$ and for the stresses σ_x (Sx), σ_y (Sy), and $\sigma_x - \sigma_y$ (Sx - Sy).

SECTION 5
SUMMARY

The focus of this investigation has been on the prediction of the fatigue life/damage of composite panels subjected to an extreme environment, i.e. to both high thermal effects (temperature and temperature gradients) and a strong acoustic transverse loading. To achieve this goal, it was necessary to accomplish the following tasks:

(i) develop an appropriate structural dynamic modeling of the panel
(ii) derive reliable approximate expressions for the statistics of the panel response to the random acoustic loading
(iii) formulate a prediction strategy of the accumulated damage in terms of the obtained statistics of the response

All three problems were successfully addressed. First, a large displacement - small strains structural dynamic model of the composite panel was accomplished by relying on the von Karman strain expressions. Further, the formulation naturally accounts for uniform temperature effects as well as the presence of in-plane and transverse temperature gradients. Finally, a higher-order displacement field was adopted to accurately capture the shear effects. Consistently with the proof of concept aspect of this Phase I effort, a simplified, one-mode approximation of the response was derived for a simply supported panel. Non-dimensionalization of the resulting equation of motion revealed that the response of different types of panels should exhibit similar characteristics and a prototypical panel was considered. The analysis of its response revealed in particular that the panel response is fairly narrowband at low sound pressure levels when the panel vibrates around its buckled states. However, as the excitation level is increased, the nonlinear effects increase as well resulting in the appearance of a subharmonic (of order 1/2) component of the response. Finally, at very high sound pressure levels, the power spectral density of the panel response exhibits a single broad peak. The nonlinearity of the displacement-stress was emphasized and a "bottoming out" effect in the stresses was observed.

The determination of reliable approximations of the statistics of the panel response to the random acoustic excitation was accomplished by relying on two separate equivalent linearization strategies. The first of these two methods seeks to approximate at best the panel response by a Gaussian process of unknown mean and variance. At low *SPL*, nonzero means are indeed found that correspond to the fluctuations around the buckled states. Above a critical *SPL*, however, this approach only yields a zero mean approximation of the "continuous" snap-through of the panel. The second equivalent linearization method relies on a mean equal to the buckled states and a representation of the panel response is obtained as the sum of zero mean fluctuations around these positions. A reliable approximation of the variance of the response was obtained, at low *SPL*, by the first of these approaches alone but, at high *SPL*, a reliable estimate of this quantity is only obtained by averaging the predictions of the two equivalent linearization strategies. Even though accurate approximations of this moment were obtained, it was shown that the exact probability density function of the panel response can accurately be matched by sums of Gaussian distributions only at low *SPL*.

The prediction of the accumulated damage in the panel was achieved by a combination of three methods: a "standard" Rayleigh approximation, a more detailed formulation taking into account the nonlinearity of the displacement-stress relation, and

finally a phenomenological modeling of the fluctuations around the buckled states and the snap-through process. When the snap-throughs occur only exceptionally, the nonlinear displacement-stress formulation yields an excellent approximation of the exact damage as estimated by an extensive simulation/rainflow analysis. However, as the sound pressure level is increased and snap-throughs start occurring, this approach underestimates the damage and the phenomenological formulation ought to be used. When the *SPL* is high enough, i.e. above the threshold at which the equivalent linearization strategy #1 fails to yield nonzero means, the average of the damages predicted by the Rayleigh and the nonlinear displacement-stress formulations was shown to be quite accurate over a broad range of sound pressure levels and S-N curve exponents.

The combination of these three different research efforts provides a solid foundation for the prediction of the fatigue life of composite and isotropic panels of various shapes, support conditions and in a wide array of extreme environments.

SECTION 6
REFERENCES

Chattopadhyay, A. and Gu H., 1994, "A New Higher-Order Plate Theory for Delamination Buckling in Composites," AIAA Journal, Vol. 32, No. 8, pp. 1709-1716.

Downing, S.D., and Socie, D.F., 1982, "Simple Rainflow Counting Algorithms," International Journal of Fatigue, pp. 31-40.

Lee, J., 1993, "Large-Amplitude Plate Vibration in an Elevated Thermal Environment," *Applied Mechanics Reviews,* Vol. 46, No. 11, Part 2, pp. S242-S254.

Lee, J., 1997, "Random Vibration of Thermally Buckled Plates: II Nonzero Temperature Gradient Across the Plate Thickness," *Applied Mechanics Reviews,* Vol. 50, No. 11, Part 2, pp. S105-S116.

Lee, J., Vaicaitis, R., Wentz, K., Clay, C., Anselmo, E., and Crumbacher, R., "Prediction of Statistical Dynamics of Thermally Buckled Composite Panels," *Proceedings of the 39th Structures, Structural Dynamics, and Materials Conference*, Long Beach, California, Apr. 20-23, 1998, Vol. 3, pp. 2539-2549, AIAA Paper 98-1975.

Kavallieratos, P.A., 1992, *Nonlinear Response of Composite Panels to Random Excitation*, Ph. D. Dissertation, Columbia University.

Lutes, L.D., and Sarkani, S., 1997, *Stochastic Analysis of Structural and Mechanical Vibrations,* Prentice-Hall.

Mignolet, M.P., 1993, "Simulation of Random Processes and Fields by ARMA Models: A Review," Chapter 7, Cheng, A.H-D., and Yang, C.Y., (Eds), *Computational Stochastic Mechanics,* pp. 149-173, Elsevier.

Moorthy, J., Mei, C., Shirahatti, U., 1995, "Numerical Simulation of Acoustically Induced Nonlinear Vibrations of a Plate with Temperature Gradient," *Proceedings of the 36th Structures, Structural Dynamics, and Materials Conference,*AIAA-95-1378-CP, New Orleans, LA, Apr. 10-13, 1844-1854.

Ng, C.F., 1988, *The Analysis of Non-Linear Dynamic Behavior (Including Snap-Through) of Postbuckled Plates by Simple Analytical Solution,* NASA Technical Memorandum 89165.

Ng, C.F., 1989, "Nonlinear and Snap-Through Responses of Curved Panels to Intense Acoustic Excitation,"*Journal of Aircraft,* Vol. 26, No. 3, pp. 281-288.

Reddy, J.N., 1987, "A Generalization of Two-Dimensional Theories of Laminated Composite Plates," *Communications in Applied Numerical Methods,* Vol. 3, No. 3, pp. 173-180.

Reddy, J.N., and Phan, N.D., 1985, "Stability and Vibration of Isotropic, Orthotropic and Laminated Plates According to a Higher-Order Shear Deformation Theory," *Journal of Sound and Vibration*, Vol. 98, No. 2, pp. 157-170.

Roberts, J.B., and Spanos, P.D., 1990, *Random Vibration and Statistical Linearization,* Wiley.

Vaicaitis, R., 1994, "Nonlinear Response and Sonic Fatigue of National Aerospace Space Plane Surface Panels," *Journal of Aircraft,* Vol. 31, No. 1, pp. 10-18.

Oppenheim, A.V., and Schafer, R.W., 1975, Digital Signal Processing, Prentice Hall.